Evolution of an Arsenal

STRUCTURAL AND FUNCTIONAL DIVERSIFICATION OF THE VENOM SYSTEM IN THE ADVANCED SNAKES (CAENOPHIDIA)*

Bryan G. Fry‡§, Holger Scheib¶‖, Louise van der Weerd, Bruce Young‡‡, Judith McNaughtan§§, S. F. Ryan Ramjan‡, Nicolas Vidal¶¶, Robert E. Poelmann**, and Janette A. Norman‡‖‖**

Venom is a key innovation underlying the evolution of advanced snakes (Caenophidia). Despite this, very little is known about venom system structural diversification, toxin recruitment event timings, or toxin molecular evolution. A multidisciplinary approach was used to examine the diversification of the venom system and associated toxins across the full range of the ~100 million-year-old advanced snake clade with a particular emphasis upon families that have not secondarily evolved a front-fanged venom system (~80% of the 2500 species). Analysis of cDNA libraries revealed complex venom transcriptomes containing multiple toxin types including three finger toxins, cobra venom factor, cysteine-rich secretory protein, hyaluronidase, kallikrein, kunitz, lectin, matrix metalloprotease, phospholipase A_2, snake venom metalloprotease/a disintegrin and metalloprotease, and waprin. High levels of sequence diversity were observed, including mutations in structural and functional residues, changes in cysteine spacing, and major deletions/truncations. Morphological analysis comprising gross dissection, histology, and magnetic resonance imaging also demonstrated extensive modification of the venom system architecture in non-front-fanged snakes in contrast to the conserved structure of the venom system within the independently evolved front-fanged elapid or viperid snakes. Further, a reduction in the size and complexity of the venom system was observed in species in which constriction has been secondarily evolved as the preferred method of prey capture or dietary preference has switched from live prey to eggs or to slugs/snails. Investigation of the timing of toxin recruitment events across the entire advanced snake radiation indicates that the evolution of advanced venom systems in three front-fanged lineages is associated with recruitment of new toxin types or explosive diversification of existing toxin types. These results support the role of venom as a key evolutionary innovation in the diversification of advanced snakes and identify a potential role for non-front-fanged venom toxins as a rich source for lead compounds for drug design and development. ***Molecular & Cellular Proteomics 7:215–246, 2008.***

It has only become evident recently that venom in snakes is a basal characteristic and that the three front-fanged venom delivery system architectures are each independent secondary derivations (1–4). In earlier schemes, the "colubrid," or "non-front-fanged," snakes were seen as a monophyletic transitional group to the presumably advanced front-fanged lineages *Atractaspis*, Elapidae, and Viperidae (*e.g.* Kardong (5)), and all front-fanged snakes were assumed to share a common ancestor. Resolution of higher order relationships revealed not only the colubrid snakes to be paraphyletic but the front-fanged snakes to be polyphyletic with viperids being one of the earliest advanced snake radiations and elapids only recently derived (1, 6).

Previous studies indicate significant morphological variation in the venom gland (7–9) and dentition of snakes (10). The fang may or may not be enlarged and can range from a solid tooth with or without grooving to an enclosed canaliculate channel as present in elapids and viperids (10). Few comparative studies of the caenophidian venom system have been performed, although West (11, 12) and Sarkar (13) described several different structural and topological features. A distinction was attempted between the venom glands of the front-fanged and non-front-fanged snakes with the glands in most non-front-fanged snakes termed "Duvernoy's glands" (7).

Similarly, very little has been revealed about the composition of venoms from advanced snake lineages other than the three clades with high pressure, hollow front-fang venom delivery systems (*Atractaspis*, elapids, and viperids). Despite accounting for the majority of the families (Fig. 1 and Ref. 6) and ~1900 of the 2500 advanced snake species, the multiple non-front-fanged families have received scant attention. Only a few studies have been undertaken, and even fewer have sequenced or bioactivity-tested individual toxins (2, 14–18).

From the ‡Department of Biochemistry and Molecular Biology, Bio21 Molecular Science and Biotechnology Institute and §§Department of Oral Medicine and Surgery, School of Dental Science, University of Melbourne, Parkville, Victoria 3010, Australia, ¶SBC Lab AG, Seebüelstrasse 26, 8185 Winkel, Switzerland, **Molecular Imaging Laboratories Leiden, MRI Facility, Departments of Anatomy and Radiology, 2300 RC, Leiden, The Netherlands, ‡‡Department of Biology, Washburn University, Topeka, Kansas 66621, ¶¶UMR 7138, Département Systématique et Evolution, Muséum National d'Histoire Naturelle, CP 26, 57 rue Cuvier, 75005 Paris, France, and ‖‖Molecular Biology, Museum Victoria, G. P. O. Box 666, Melbourne, Victoria 3001, Australia

Received, March 2, 2007, and in revised form, September 10, 2007
Published, MCP Papers in Press, September 17, 2007, DOI 10.1074/mcp.M700094-MCP200

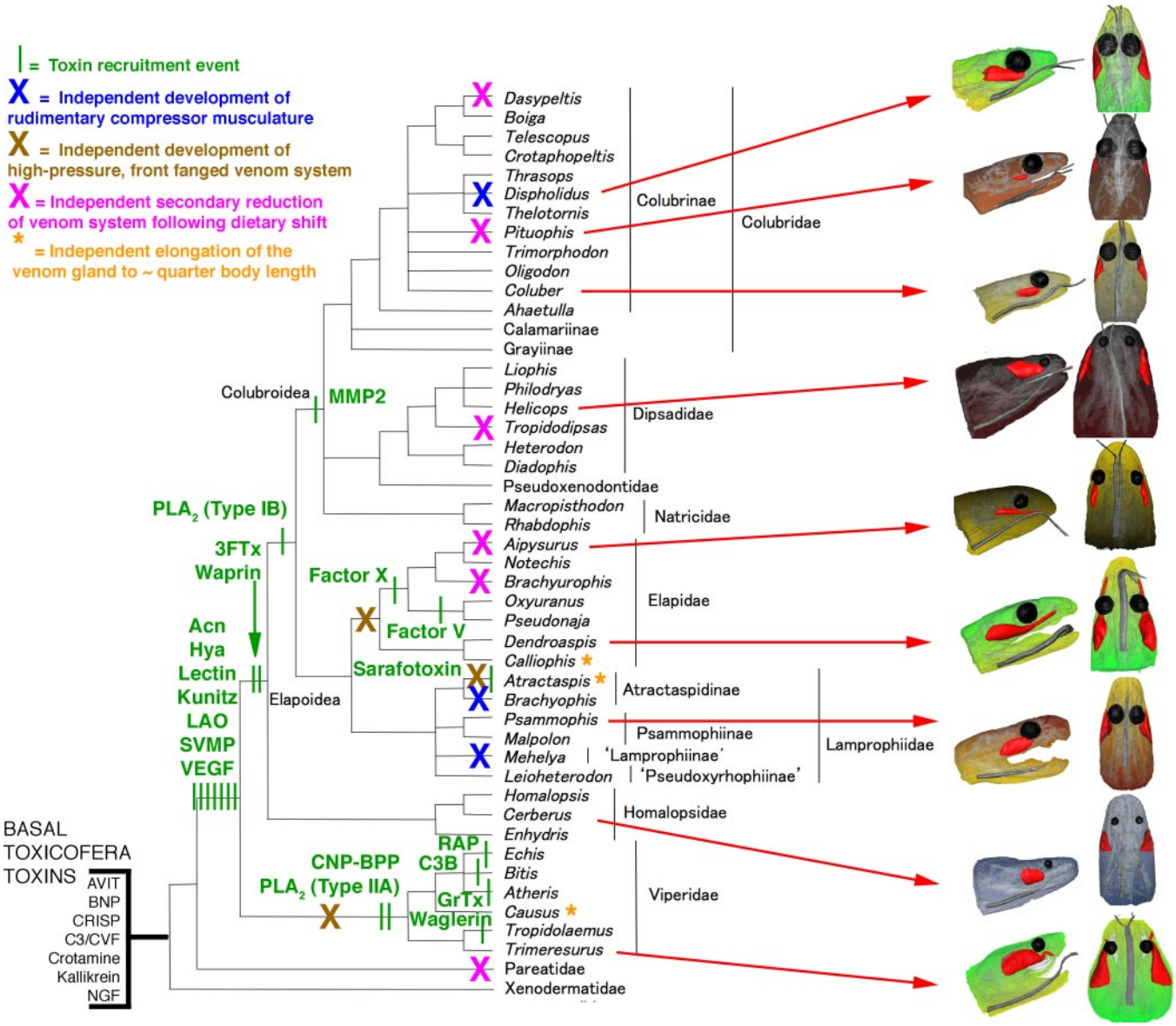

FIG. 1. **Cladogram of evolutionary relationships of advanced snakes (1, 6, 58–61) showing relative timing of toxin recruitment events and derivations of the venom system.** MRI images are shown for representatives. *Acn*, Acetylcholine esterase; *LAO*, L-amino oxidase; *C3B*, FAMC3B cytokine; *CNP-BPP*, c-type natriuretic peptide-bradykinin-potentiating peptide; *GrTx*, glycine-rich toxin; *Hya*, hyaluronidase; *RAP*, renin-like aspartic protease; *VEGF*, vascular endothelial growth factor.

Studies of the first full-length toxins from non-front-fanged snakes were revealing, particularly the isolation and characterization of a potently neurotoxic three-finger toxin (3FTx)[1] from the colubrid snake *Coelognathus radiatus* (2). This toxin type had long been considered the hallmark of elapid venoms and had been the subject of intense study (19). Follow-up molecular phylogenetic studies demonstrated the shared origin of 3FTx and other toxin types across the entire advanced snake radiation (3).

In view of the homology of the venom toxins and toxin-secreting glands of all advanced snakes, the fact that Duvernoy's glands represented a primitive condition and that the derived glands of the front-fanged snakes were independently evolved from these, the distinction between Duvernoy's glands and venom glands was revealed to be an artificial one that impeded the understanding of the evolution of the venom apparatus of snakes. For this reason, the term Duvernoy's gland was abandoned, and the term "venom gland" was used for the toxin-secreting oral glands of all snakes regardless of

[1] The abbreviations used are: 3FTx, three-finger toxin; CRISP, cysteine-rich secretory protein; SVMP, snake venom metalloprotease; ADAM, a disintegrin and metalloprotease; BLAST, Basic Local Alignment Search Tool; 3D, three-dimensional; SPDBV, Swiss-PdbViewer; MRI, magnetic resonance imaging; T, tesla; CVF, cobra venom factor; MMP, matrix metalloprotease; PLA_2, phospholipase A_2; CRD, cysteine-rich domain.

the degree of anatomical specialization in the venom delivery apparatus (14).

It has been shown previously that snake venoms evolve via a process by which a gene encoding for a normal body protein, typically one involved in key regulatory processes or bioactivity, is duplicated, and the copy is selectively expressed in the venom gland (20). The newly created toxin type evolves via the birth-and-death model of protein evolution in which a toxin multigene family is created by further gene duplication events followed by the deletion of some copies and conversion of others to non-functional copies or pseudogenes (19).

In addition to gene duplication, mutation is an important process that generates a tremendous diversity of venom toxins within these multigene families. The newly created toxin multigene families preserve the molecular scaffold of the ancestral protein but modify key functional residues at the tips of loops to acquire a myriad of newly derived activities (19, 20). Other mutations can include the selective expression of a particular domain, such as the expression of the disintegrin domain from snake venom metalloprotease, ADAM-type (SVMP/ADAM) toxins in viperid venoms (21). These toxins have an unusual combination of precise specificity and extreme potency, characteristics that make them particularly amenable for use as investigational ligands or as leads for drug design and development (22–24).

In this study we used a multidisciplinary approach to (*a*) characterize the venom transcriptomes of representative caenophidian snakes, (*b*) determine the timing of toxin recruitment events and patterns of toxin diversification, and (*c*) characterize changes in the venom delivery architecture. From comparison with the more widely studied elapids and viperids, we determined whether there are significant structural or functional differences in the evolution of the venom system and their associated toxins in the poorly characterized non-front-fanged caenophidian snakes.

MATERIALS AND METHODS

Species Studied and Molecular Phylogeny of Advanced Snakes—A total of 107 species representing each of the major lineages of advanced snakes were included in the study and examined using one or more of the following techniques: clone sequencing of cDNA libraries, gross dissection and examination of dentition, histology of venom glands and ducts, and magnetic resonance imaging (see "Appendix I" for details). In most cases different individuals were used as a source of material for each of these analyses.

cDNA Library Construction and Analysis—RNA was isolated from venom glands of 13 species spanning the full taxonomical diversity (10 non-front-fanged snakes, one elapid, and two viperids; see "Appendix I") using the Qiagen RNeasy Midi kit with subsequent selection of mRNAs using the Oligotex Midi kit. cDNA libraries were constructed using the Clontech Creator SMART cDNA Library Construction kit and transformed into One Shot Electrocompetent GeneHogs (Invitrogen) as described previously (4). Isolation and sequencing of inserts was undertaken at the Australian Genome Research Facility using BDTv3.1 chemistry with electrophoretic separation on an AB330xl. Up to 384 colonies were sequenced per library, inserts were screened for vector sequences, and those parts were removed prior to analysis and identification. Toxin sequences were identified by homology of the translated cDNA sequences with previously characterized toxins using a BLAST search of the Swiss-Prot protein database (www.expasy.org/tools/blast/).

Molecular Modeling of Toxins—3D models for caenophidian toxins were generated based on the assumption that homologous proteins share similar 3D structures (25). In other words, the three-dimensional structure of a target protein can be modeled if its sequence is homologous to at least one template protein whose 3D structure has been determined experimentally by applying either x-ray or NMR techniques (26). In this work aligning the protein sequences of target and template(s) was carried out in SPDBV (27), and the initial alignments were refined manually. From these alignments 3D models were built directly in SPDBV applying the "Build Preliminary Model" option, which is disabled in the currently distributed public version of the software. Loops were built by scanning a database of known loop structures using the same software, and suitable specimens were selected after visual inspection. The enthalpy of the resulting models was minimized applying two times 200 steps of Steepest Descent minimization. Finally the quality of each model structure was assessed in iMolTalk (28), and a Van der Waals surface was calculated in MolMol (29). In MolMol electrostatic potentials were calculated applying the "simplecharge" command and mapped on the model structure surface. The families of venom proteins were analyzed by superimposing the structures in SPDBV (27), and conserved and variable structural regions were identified. In the molecular modeling of representative proteins, blue surface areas indicate positive charges, red surface areas indicate negative charges, and model pairs show sides of the protein rotated by 180°.[2]

Molecular Phylogeny of Toxin Sequences—Molecular phylogenetic analyses of toxin transcripts were conducted using the translated amino acid sequences. Comparative sequences from other venomous reptiles and outgroups were obtained through BLAST searching (www.expasy.org/tools/blast/) using representative toxin sequences. To minimize confusion, all sequences obtained in this study are referred to by their GenBank™ accession numbers (www.ncbi.nlm.nih.gov/sites/entrez?db=Nucleotide), and sequences from previous studies are referred to by their UniProt/Swiss-Prot accession numbers (www.expasy.org/cgi-bin/sprot-search-ful). Resultant sequence sets were aligned using the program ClustalX followed by visual inspection for errors. When presented as sequence alignments, the leader sequence is shown in lowercase, the prepro region is underlined, cysteines are highlighted in black, and functional residues are in bold. Datasets were analyzed using Bayesian inference implemented on MrBayes, version 3.0b4. The analysis was performed by running a minimum of 1×10^6 generations in four chains and saving every 100th tree. The log likelihood score of each saved tree was plotted against the number of generations to establish the point at which the log likelihood scores of the analysis reached their asymptote, and the posterior probabilities for clades were established by constructing a majority rule consensus tree for all trees generated after the completion of the burn-in phase.[3]

Gross Dissection and Analysis of Dentition—Gross dissection was performed on freshly euthanized and formalin-fixed specimens to document the relative size and position of the venom gland and associated skeletal musculature. Features of the maxillary dentition were scored using data from a previous study (10) in which five morphological states were defined: 1) smooth surface and no en-

[2] Homology model coordinates can be obtained from H. Scheib. E-mail: holger@moltalk.org.

[3] Sequence alignments can be obtained from B. G. Fry. E-mail: bgf@unimelb.edu.au.

TABLE I
Toxin types recovered from mRNA transcript sampling
CRI, CRISP; Fac X, Factor X; Ka, kallikrein; Ku, kunitz; Lec, lectin; NGF, nerve growth factor; Wap, waprin.

	3FTx	CRI	CVF	Fac X	Ka	Ku	Lec	NGF	PLA_2 Type IA	PLA_2 Type IB	SVMP	Wap
Colubridae											X	
D. typus	X	X									X	
T. dhara	X	X				X					X	
T. jacksonii	X						X				X	X
T. biscutatus	X	X								X		
Dipsadidae												
L. poecilogyrus	X	X					X				X	X
P. olfersii		X			X	X	X				X	X
Elapidae												
O. microlepidotus	X	X		X		X				X		X
Homalopsidae												
E. polylepis	X						X				X	X
Natricidae												
R. tigrinus		X										X
Psammophiinae												
P. mossambicus	X										X	
Pseudoxyrhophiinae												
L. madagascariensis	X	X	X				X				X	
Viperidae												
Azemiops feae								X	X			
C. rhombeatus		X			X		X		X		X	

closed venom canal, 2) no enclosed venom canal and surface with shallow furrow, 3) deep groove running the majority of the length of the tooth, 4) deep groove present but restricted to less than half the length of the tooth, and 5) enclosed venom canal.

Histological Analysis—Histological sections were prepared from the intact head and the excised venom delivery system. Whole heads were removed, and a cut was made to the underside to allow fast penetration of the fixative (10% neutral buffered formalin). After a minimum of 2 days excess tissue was removed, and specimens were immersed in Kristensen's decalcification solution and placed on a rotor for up to 3 weeks (depending on the size of the head). Before processing the heads were bisected longitudinally for cutting transversely, at 3 μm, in two separate blocks. The processing schedule was: 10% formalin, 2 h; absolute ethanol, 4 $\times$ 1 h; Histolene, 3 $\times$ 1 h; paraffin wax, 2 $\times$ 90 min. The sections were taken every 100 μm, and matching sections were stained with periodic acid-Schiff stain and Masson's trichrome stain. In other specimens, the venom gland, venom duct, and the adjacent bony and muscular tissue were excised and placed in decalcifying solution (Cal-Ex, Fisher) for 72–168 h. Each sample was dehydrated and cleared through a progressive ethanol series and Cyto-Sol (Fisher) prior to embedding in Paraplast (Fisher). Serial sections were cut at 10–12 μm. All species were sectioned in the frontal plane; when available, the contralateral venom delivery system was sectioned either parasagittally or transversely. Sections were stained using a variant of Van Gieson's stain, which provides clear distinction between connective tissue, muscle, and epithelium, or with hematoxylin and eosin.

Magnetic Resonance Imaging—Magnetic resonance imaging (MRI) was used to examine the three-dimensional shape and internal anatomy of the venom glands. Formalin-ethanol-fixed heads were first submersed in Fomblin (Solvay Solexis) to prevent air artifacts. Depending on head size, imaging was performed on either 9.4-T (small/medium) or 17.6-T (large) vertical 89-mm-bore systems (Bruker BioSpin, Rheinstetten, Germany) with a Bruker Micro2.5 gradient system of 1 T/m and transmit/receive birdcage radiofrequency coil with diameter of 10–30 mm. Bruker ParaVision 3.0 software was used for image acquisition. Anatomical images were acquired using a 3D gradient echo sequence. The field of view and matrix were varied to fit the individual samples, resulting in voxel sizes between $(40)^3$ and $(70)^3$ mm^3. Imaging parameters were: echo time = 8 ms; repetition time = 40 ms; flip angle, 20°; four to eight averages; total scan time between 3 and 9 h per sample, depending on size and resolution. Image segmentation of the glands was performed manually in Amira 4.1 (Mercury Computer Systems Inc.), and 3D surface renderings were generated for all species.

RESULTS

Isolation and Characterization of Venom Toxin Transcripts—Analysis of venom gland cDNA from non-front-fanged snake libraries revealed the presence of transcripts with homology to previously characterized venom toxins from front-fanged snakes and venomous lizards (helodermatids and varanids) (Tables I and II). Transcripts sequenced were 3FTx (Figs. 2 and 3), C3/cobra venom factor (CVF) (Fig. 4), cysteine-rich secretory protein (CRISP) (Figs. 5 and 6), hyaluronidase (Fig. 7), kallikrein (Figs. 8 and 9), kunitz (Figs. 10 and 11), lectin (Figs. 12 and 13), matrix metalloprotease (MMP) (Fig. 14), phospholipase A_2 (PLA_2) Type IB (Fig. 15), SVMP/ADAM (Figs. 16, 17, and 18), and waprin (Fig. 19). Transcripts of five of these toxin types were also recovered from the cDNA libraries of the representative elapid *Oxyuranus microlepidotus* (3FTx, CRISP, kunitz, and waprin) and the viperid *Causus rhombeatus* (kallikrein).

Alignment of the translated amino acid sequences revealed extensive variation in the molecular structure of the transcripts for most toxin types. There was less amino acid sequence divergence in C3/CVF, CRISP, hyaluronidase, kunitz, PLA_2 (Type IB), and MMP toxins than in the much more variable

TABLE II

Transcripts from non-front-fanged snakes and previously characterized basal and derived bioactivities from elapid or viperid venoms (19)

VWF, von Willebrand factor; GP, glycoprotein.

Toxin type	Bioactivities
3FTx	Ancestral toxic activity of α-neurotoxicity, antagonistically binding to the nicotinic acetylcholine receptor; α-neurotoxicity greatly potentiated by the deletion of the second and third ancestral cysteines. Functional derivations include binding to the postsynaptic muscarinic acetylcholine receptors, presynaptic neurotoxic action upon the L-type calcium channels, cytotoxic interactions, acetylcholinesterase inhibition, and others.
C3/CVF	Ancestral activity of unregulated activation of the complement cascade causing rapid and significant problems such as anaphylactic-type problems and/or tissue damage via hemolysis/cytolysis. Derived activities not currently documented.
CRISP	Ancestral activity of paralysis of peripheral smooth muscle and induction of hypothermia due to the action upon voltage-gated Ca^{2+} channels and resultant blockage of K^+-induced contraction. Derived activities include blockage of cyclic nucleotide-gated calcium channels.
Hyaluronidase	Venom spreading factor.
Kallikrein	Ancestral toxic activity of increase of vascular permeability and production of hypotension in addition to stimulation of inflammation. Derived activities affect the blood, particularly targeting fibrinogen.
Kunitz	Ancestral toxic activity of inhibition of circulating plasma serine proteases. Derivations include inhibition of plasmin and thrombin and the blockage of L-type calcium channels. Structural derivatives form part of neurotoxic complexes with PLA_2 molecules.
Lectin	Ancestral toxic activity of inhibition of platelet aggregation mediated by galactose binding. Derivations include stimulation of platelet aggregation (binding GPVI, GPIb, GPIa/IIa, or VWF), platelet aggregation inhibition (binding GPIb or GPIa/IIa), or anticoagulant actions by binding blood factors IX and X.
PLA_2 (Type IB)	Ancestral toxic activity of lipase activity resulting in inflammation and tissue destruction. Presynaptic neurotoxicity is a basal derivation.
SVMP/ADAM	Ancestral toxic activity of tissue edema and necrosis. Prothrombin activation is a basal derivation. In Viperidae venoms, proteolytic cleavage of C-terminal domains results in a myriad of other activities including direct acting fibrinolytic activity; liberated disintegrin domain inhibits platelets via GPIIb/IIIa integrin receptor.
Waprin	Only antimicrobial activities currently described.

3FTx, kallikrein, lectin, SVMP/ADAM, and waprin toxins. For most toxin types multiple transcripts containing significant molecular variations were also isolated from individual cDNA libraries; this is a characteristic previously attributed to accelerated diversification in these toxin multigene families (19). cDNA sequencing revealed numerous transcripts in the venom glands of non-front-fanged snakes that preserve the key amino acids essential for a particular bioactivity and potentially represent the mRNA precursors of functional proteins.

Reflective of sequence variation of proteins in the CRISP family, its members have been found to interact with different target proteins, *i.e.* cyclic nucleotide-gated ion channels as well as L-type Ca^{2+} and BK_{Ca} K^+ channels (30–32). Binding to the respective channels is speculated to be a general property of CRISP and was attributed to a predominantly hydrophobic cavity involving residues from both domain PR-1 and cysteine-rich domain (CRD), whereas specific channel block supposedly is taking place with residues of CRD (30–35). Six amino acids were identified for the calcium channel blocker Triflin (Protein Data Bank code 1WVR (30)) to bind to ion channels (numbering according to Triflin): Glu-44, Tyr-54, Ser-65, Tyr-125 (all four in PR-1), Thr-184, and Arg-185 (both in CRD). An additional four amino acids were conserved and postulated to affect ion channel function of this neurotoxin. They are all located in CRD: Phe-189, Leu-195, Tyr-205, and Phe-215. However, this work reveals that none of these 10 positions is conserved throughout the CRISP toxin family. Even more so our *in silico* studies could not confirm suggested functional motifs, namely EX_2F and DVF, at least as a general principle of CRISP. Differences in CRISP function of toxic venom proteins and the non-toxic representative from mouse are subtle and likely to be found in CRD, *i.e.* Leu-220 and Leu-230 (numbering according to mouse; Fig. 5). The promiscuous susceptibility of CRISP toward different ion channels is reflected in their high degree of sequence variation. In the absence of obvious sequence and structure differences between toxic and non-toxic specimens (Figs. 5 and 6) it will be necessary to acquire further data on the function of the CRISP family members to identify the functionally discriminating amino acids.

The hyaluronidase transcript sequenced from *Liophis poecilogyrus* showed significant sequence similarity to those sequenced from viperid venoms (36), and the snake sequences all formed a clade (Fig. 7). Kallikrein transcripts isolated from *Philodryas olfersii* retained residues essential for the potent hypotensive action mediated by the liberation of bradykinin from kininogen (Fig. 8).

Kunitz-type toxins belong to the superfamily of bovine pancreatic trypsin-like inhibitors. Although they share the same overall 3D fold, their antitrypsin activity may vary. It has been long known that the residue in the so-called P1 site of the trypsin inhibitor is positively charged (arginine, lysine, or histidine), whereas this residue in a chymotrypsin inhibitor usually is large and hydrophobic (leucine, phenylalanine, tyrosine,

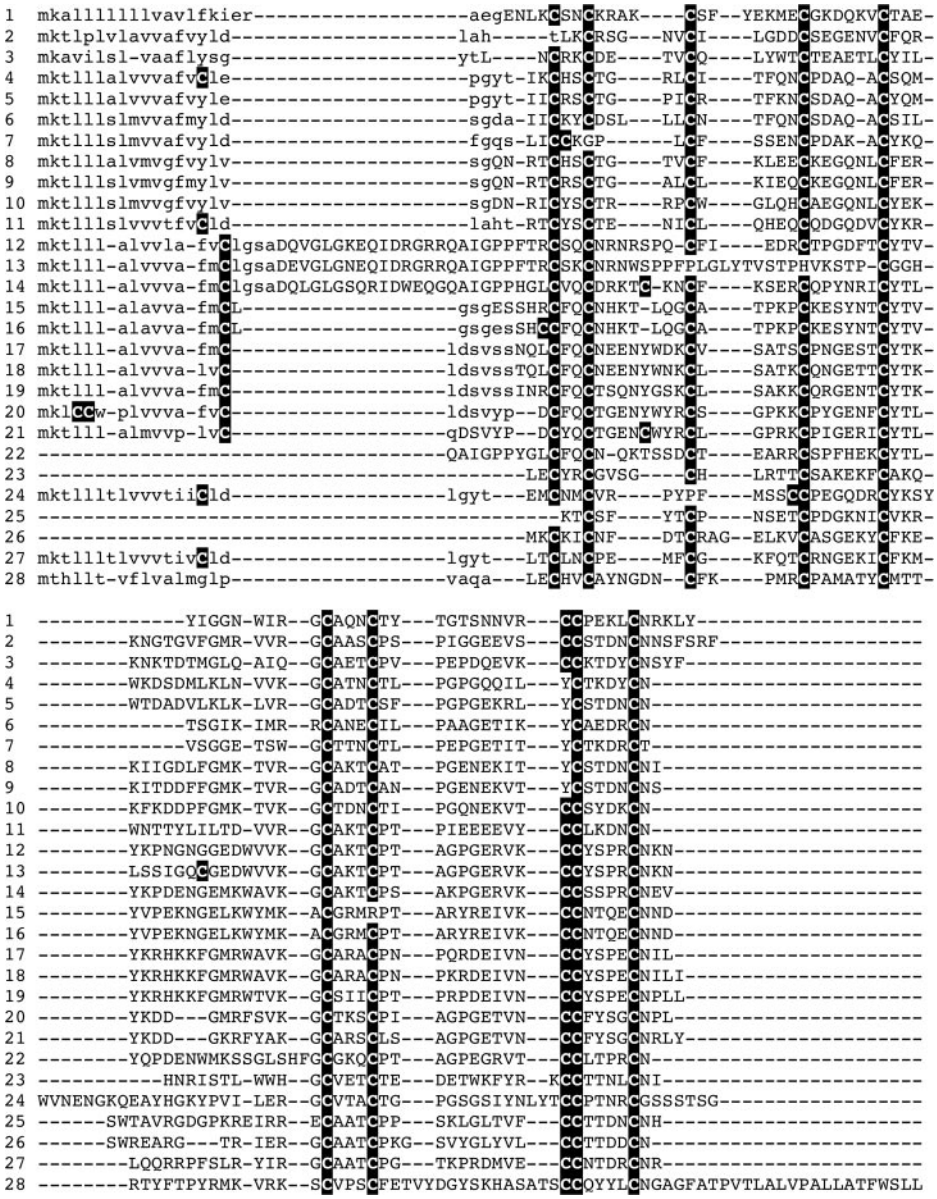

FIG. 2. **Sequence alignment of representative 3FTx.** Species shown are *E. polylepis* (*1*, EU029668), *P. mossambicus* (*2*, EU029669), *L. poecilogyrus* (*3*, EU029670; *6*, EU029672; *7*, EU029673), *T. dhara* (*4*, EU029671), *D. typus* (*5*, EU029674; *9*, EU036636; *17*, EU029681; *19*, EU029683), *T. jacksonii* (*8*, EU036635; *18*, EU029682; *20*, EU029684; *21*, EU029685), *T. biscutatus* (*10*, EU029675; *12*, EU029677; *13*, EU029678), *Leioheterodon madagascariensis* (*11*, EU029676), *T. dhara* (*14*, EU029686; *15*, EU029679; *16*, EU029680), *C. radiatus* (*22*, P83490), *Dendroaspis jamesonii* (*23*, P25682), from *B. multicinctus* (*24*, Q9PW19; *25*, Q9YGJ0), *Bungarus candidus* (*26*, P81783), and *Naja sputatrix* (*27*, Q9W7I3). Also included is the representative non-toxin peptide brain α-neuropeptide (*28*, Q9WVC2) from *Mus musculus*.

or asparagine) (37). From the multiple sequence alignment presented in Fig. 10 it can be concluded that kunitz-type toxins from *P. olfersii*, *Ophiophagus hannah*, *Naja naja*, and *Bungarus multicinctus* are likely to inhibit chymotrypsin, whereas the others putatively are trypsin inhibitors. Our 3D modeling efforts showed that the kunitz toxins vary, *i.e.* in the length of their C- but also their N-terminal tails (Figs. 10 and 11). The N-terminal tail is held in place by formation of two disulfide bonds involving the first and sixth as well as the second and fourth cysteines. The inhibitory residues are solvent-exposed and reside in a long surface loop immediately after the second cysteine, which indicates that the position of these residues is rather conserved among kunitz toxins (Figs. 10 and 11). Therefore, changes in polarity and charge are expected to affect the physicochemical properties of this region.

Within the lectin toxins, variation of a key tripeptide motif has been shown to have significant impact upon functionality (38) with EPN conferring mannose binding ability, whereas QPD confers galactose binding. In this study, both were obtained as well as new variants of this motif containing EAP, QAP, and LTD (Figs. 12 and 13). The EPN motif appears to be basal, whereas the QPD motif is an early emerging variant, and the other variants evolved subsequently at different times during the evolution of the animals themselves. The viper venom-specific heterodimeric forms have lost this motif entirely.

A novel MMP toxin had been reported previously from the venom of the lethal natricid snake *Rhabdophis tigrinus* (39). However, only a very small fragment was obtained so the MMP-subtype relationship remained unclear. In this study, a full-length MMP was obtained from the *L. poecilogyrus* library

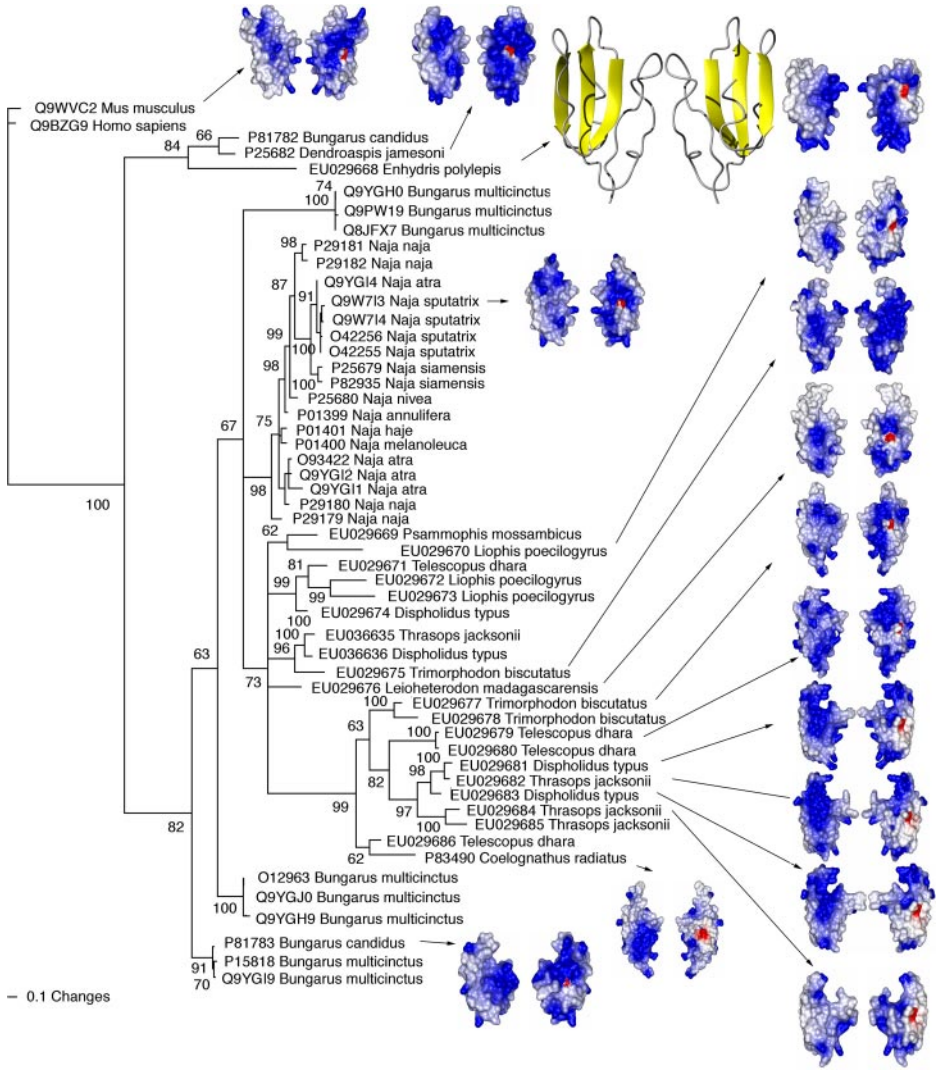

FIG. 3. **Bayesian molecular phylogeny of 3FTx.** The outgroup is the non-toxic brain α-neuropeptide (Q9WVC2) from *M. musculus*. The ribbon model of EU029668 *E. polylepis* shows β-strands in *yellow*.

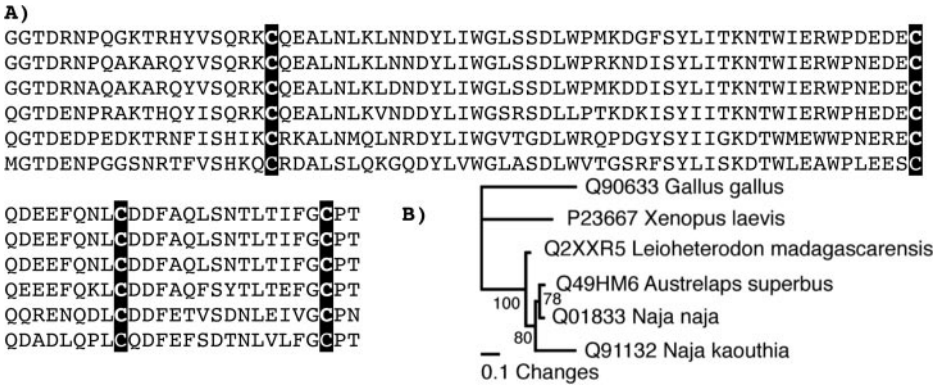

FIG. 4. **Molecular evolution of C3/CVF toxins.** *A*, partial sequence alignment of the representative toxin forms shown from *top* to *bottom*: Q2XXR5 from *L. madagascariensis*, Q49HM6 from *Austrelaps superbus*, Q01833 from *N. naja*, and Q91132 from *Naja kaouthia* as well as the non-toxin forms P23667 from *Xenopus laevis* and Q90633 from *Gallus gallus*. *B*, Bayesian molecular phylogenetic analysis of representative toxin and non-toxin body forms. Outgroups are the non-toxin sequences P23667 *X. laevis* and Q90633 *G. gallus*.

and was shown to be closest to MMP2 (Fig. 14) rather than showing the MMP9 relationship hypothesized in the previous *R. tigrinus* study.

A Type IB PLA_2 transcript was isolated from *Trimorphodon biscutatus* that retained not only the ancestral pancreatic loop but also the catalytic diad residues histidine and aspartate as well as two conserved tyrosine residues that together with structural water form the catalytic center (Fig. 15). This toxin is most likely responsible for conferring the presynaptic neurotoxicity observed for this venom (40). The electrostatic surfaces of PLA_2 IB clearly indicate the overall similarity of the five toxins studied both in terms of size and shape as well as

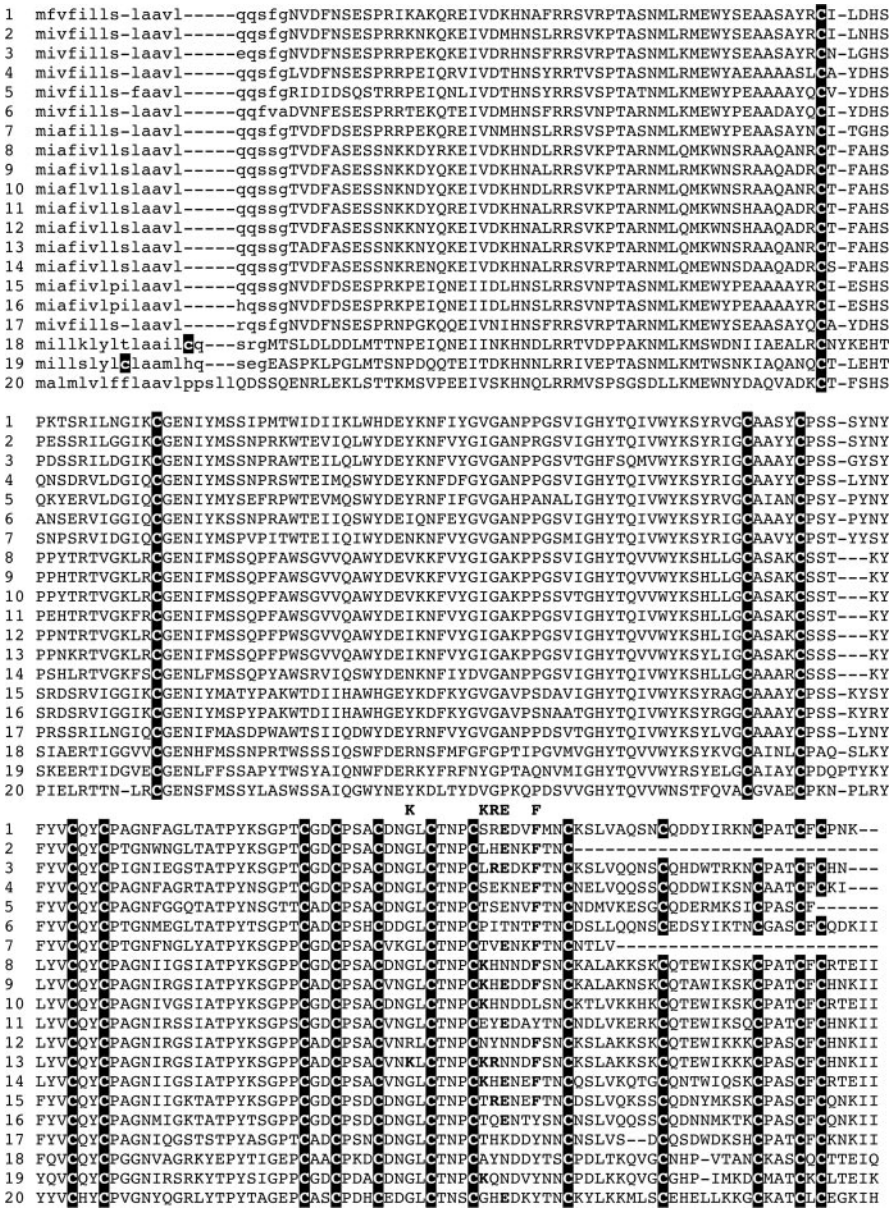

FIG. 5. **Sequence alignment of representative full-length (unless otherwise indicated) CRISP toxins.** *1*, Q2XXQ5 from *D. typus*; *2*, partial sequence Q2XXP5 from *T. dhara*; *3*, partial sequence Q2XXP4 from *T. biscutatus*; *4*, partial sequence Q2XXP7 from *P. olfersii*; *5*, partial sequence Q2XXQ0 from *L. poecilogyrus*; *6*, Q2XXQ3 from *E. polylepis*; *7*, partial sequence Q2XXQ1 from *L. madagascariensis*; *8*, Q2XXP9 from *O. microlepidotus*; *9*, Q3SB03 from *Hoplocephalus stephensii*; *10*, Q3SB05 from *P. textilis*; *11*, Q8UW11 from *L. curtus*; *12*, Q8AVA3 from *Pseudechis porphyriacus*; *13*, Q8AVA4 from *Pseudechis australis*; *14*, Q8JI38 from *Laticauda semifasciata*; *15*, Q8JI39 from *Trimeresurus flavoviridis*; *16*, P79845 from *P. mucrosquamatus*; *17*, Q8JGT9 from *R. tigrinus*; *18*, Q2XXP1 from *Varanus varius*; *19*, Q91055 from *H. horridum*; *20*, the non-toxin representative Q91XA3 from *M. musculus*.

with regard to the physicochemical properties. It can be concluded that all PLA_2 IB toxin specimens exhibit very similar neurotoxic function.

The SVMP/ADAM sequences were shown to be of the PIII type, consistent with previously reported fragments from *Dispholidus typus* (41). Numerous transcripts were also recovered with significant variations including changes in the number and spacing of cysteine residues and large scale deletions. Caenophidian 3FTx, lectin, MMP, SVMP, and waprin transcripts were all characterized by changes in ancestral cysteines in addition to the evolution of new cysteines (Figs. 2, 12, 16, 17, and 19). In contrast, transcripts of the caenophidian C3/CVF, CRISP, hyaluronidase, kallikrein, kunitz, and PLA_2 Type IB toxins preserved the ancestral cysteine numbers and spacing (Figs. 4, 5, 8, 10, and 15). Large deletions were detected in transcripts of the lectin and SVMP/ADAM toxins. Multiple transcripts of a deleted form of the lectin toxin were isolated from *Enhydris polylepis* (Fig. 12) in which a large stretch of residues including an ancestral cysteine is deleted, leaving a free cysteine, potentially facilitating dimerization. Another lectin toxin version from the *E. polylepis* cDNA (again for which multiple transcripts were obtained) had a significant change in sequence to the second half of the protein as a consequence of a frameshift mutation. The resulting new transcript contains overall four cysteine bonds and therefore may fold into a stable, bioactive molecule. A major truncation was detected in transcripts of the SVMP/ADAM toxins isolated from *Psammophis mossambicus* (Fig. 16). These transcripts consisted solely of the propeptide

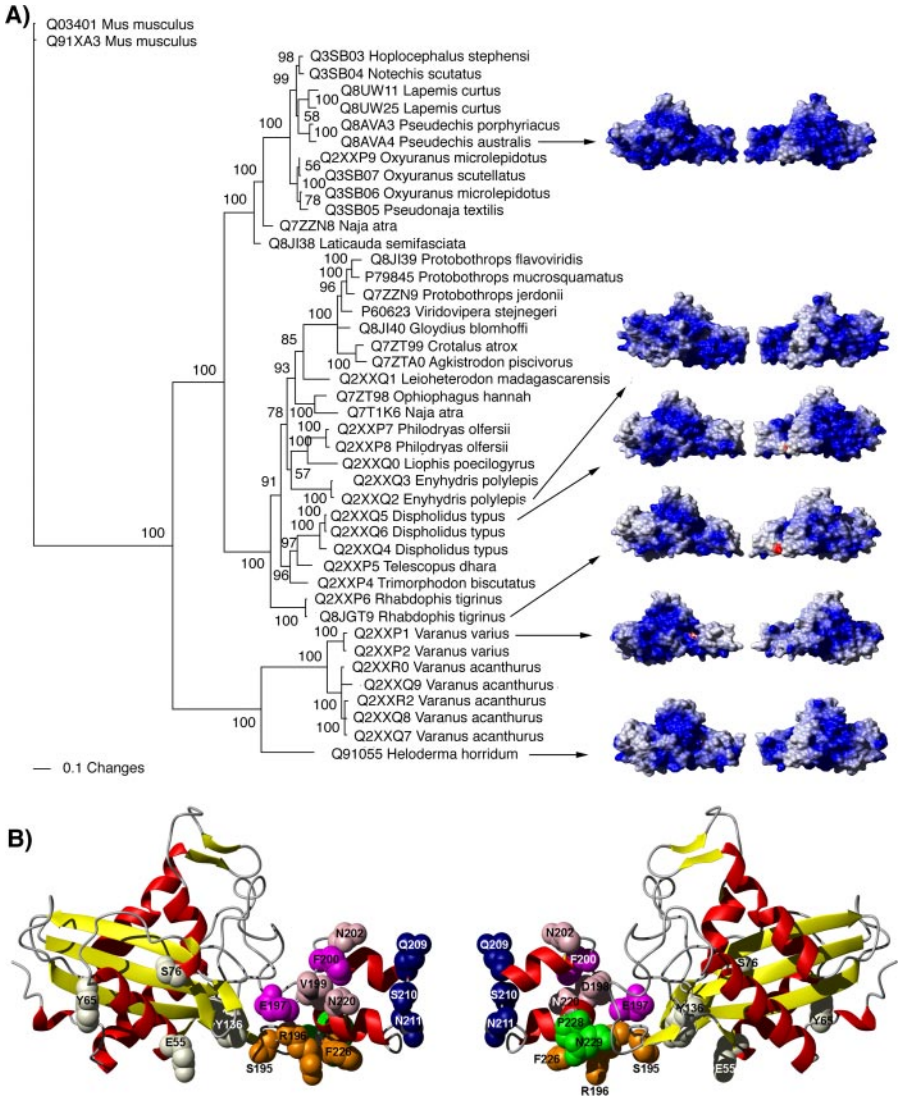

FIG. 6. *A*, Bayesian molecular phylogeny of CRISP toxins. Outgroups are non-toxin forms Q034O1 and Q91XA3 from *M. musculus*. *B*, ribbon view of Q2XXQ5 from *D. typus*. α-Helices are in *red*, and β-strands are in *yellow*. Residues postulated to bind to ion channels (without blocking them) are in *white* (Glu-55, Tyr-65, Ser-76, and Tyr-136 in PR-1; Ser-195 and Arg-196 in CRD); Ser-195 and Arg-196 are colored *orange* because they are part of a putative ion channel blocking site. The EX_2F motif is in *magenta*, *i.e.* Glu-197 and Phe-200. Channel blocking motif hypothesized in this study is shown: part I in *pink* containing Val-199 and Phe-200 (of the DVF, EX_2F motifs) but also Asn-202 and Asn-220; part II in *blue* containing Gln-209, Ser-210, and Asn-211; part III in *orange* consisting of Ser-195, Arg-196, and Phe-226; and part IV in *green* consisting of the C-terminal tail Pro-228 and Asn-229.

region normally post-translationally cleaved from the functional enzymatic region, and some isoforms had evolved new cysteines within this domain.

Structural Variation of the Venom System—The combination of MRI, histological analysis, gross dissection, and examination of dentition revealed extensive variations in the relative size of the venom gland and lumen and variation in the course of the venom duct (Figs. 1, 20, and 21 and see "Appendix II"). Large venom glands, similar in size to those of some elapids, were found in representatives from each of the different non-front-fanged families, such as the colubrid snake *Telescopus dhara*, the homalopsid snake *Cerberus rynchops*, the psammophiine snake *P. mossambicus*, and the dipsadid snake *Helicops leopardinus*. The lethal colubrid snake *D. typus* had the most robust glands of all non-front-fanged snakes studied. In contrast, the venom glands of two colubrid snakes (*Pituophis guttatus* and *Dasypeltis scabra*) were found to be greatly atrophied as was that of the pareatid *Pareas carinatus*. The course of the venom ducts ranged from nearly craniad in the elapid and viperid to varying degrees of medial or craniomedial in the non-front-fanged species.

In histological analyses the serous (protein-secreting) section of the venom gland was isolated and easily distinguished from the mucus-secreting supralabial glands of all species. In the majority of the taxa examined the venom duct was lined with a combination of stratified squamous and mucoid cells. The relative amount of mucoid cells was far more variable within the non-front-fanged snakes; mucoid cells were absent in some taxa (*e.g. Diadophis punctatus*). In *Atractaspis bibronii* the radially arranged secretory tubules have a mucoid section at their opening into the central lumen. Irrespective of the epithelial lining, the majority of the taxa examined had a localized expansion of the venom duct, termed a venom vestibule. A venom vestibule was located adjacent to the fang sheath of all front-fanged species as well as many non-front-fanged snakes. However, unique among the non-front-fanged

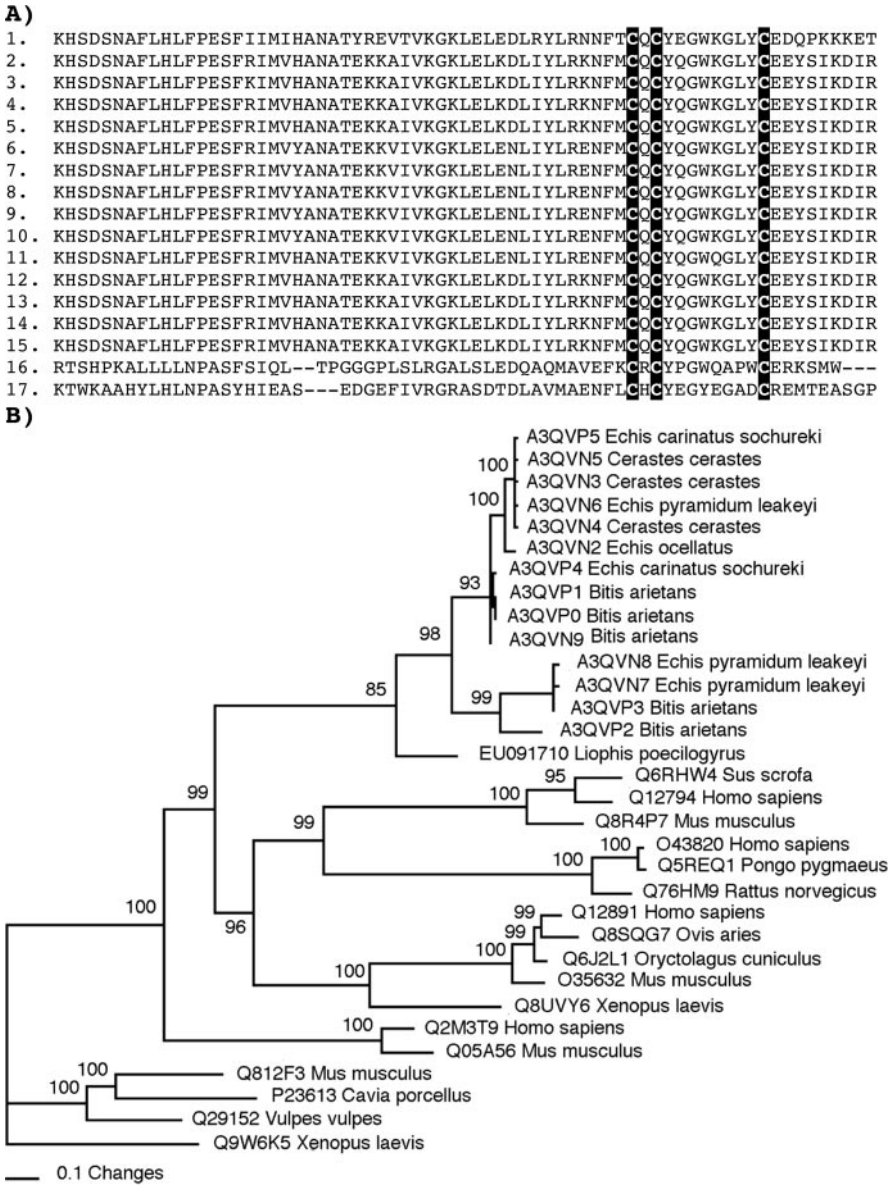

FIG. 7. **Hyaluronidase.** *A*, partial sequence alignment of toxin sequences. *1*, EU091710 from *L. poecilogyrus*; *2*, A3QVP2; *5*, A3QVP3; *13*, A3QVP1; *14*, A3QVP0; *15*, A3QVN9, all from *Bitis arietans*; *3*, A3QVN8; *4*, A3QVN7; *6*, A3QVP5; *9*, A3QVN6, all from *Echis pyramidum leakeyi*; *7*, A3QVN5; *8*, A3QVN3; *10*, A3QVN4, all from *Cerastes cerastes*; *11*, A3QVN2 *Echis ocellatus*; *12*, A3QVP4 from *Echis carinatus sochureki*. Also shown are the representative non-toxins: *16*, Q12794 from *Homo sapiens*; *17*, Q05A56 from *M. musculus*. *B*, Bayesian molecular phylogeny; the outgroup is Q9W6K5 from *Xenopus laevis*.

snakes was the presence of a venom vestibule located along the medial surface of the venom gland. The proximal portion of the venom duct was septate in the front-fanged taxa and generally ovoid and largely free of surrounding connective tissue in the non-front-fanged taxa. In a few of them (most notably in *D. typus*, *Stenorrhina freminvillei*, and *Thelotornis capensis*) the venom duct was more crenate in cross-section and was surrounded by concentric layers of connective tissue suggestive of pressure regulation.

The greatest level of morphological variation was found in the topographical relationship between the venom duct and the fang. In some non-front-fanged taxa (*e.g. Heterodon*) the venom duct opens directly into the oral cavity rather than to the lumen of the fang sheath and the surface of the fang. In other cases the venom duct courses directly to the fang sheath with no venom vestibule located at the juncture between these two structures as it is in all front-fanged taxa. Most commonly in non-front-fanged snakes the venom duct opened both into the fang sheath and directly to the roof of the mouth immediately adjacent to the fang sheath; this dual opening was achieved by the venom duct, or in some cases the associated venom vestibule, paralleling the long axis of the fang sheath forming a prominent diverticulum. In a few non-front-fanged taxa there was a secondary venom duct that arose from the distal portion of the fang sheath and extended peripherally to contact the roof of the mouth. Combining information for the different structural features revealed the non-front-fanged snakes to possess a highly variable venom system architecture with all combinations of epithelial lining, venom vestibule, and venom duct topography identified (see "Appendix II").

The maxillary dentition was also revealed to be extremely

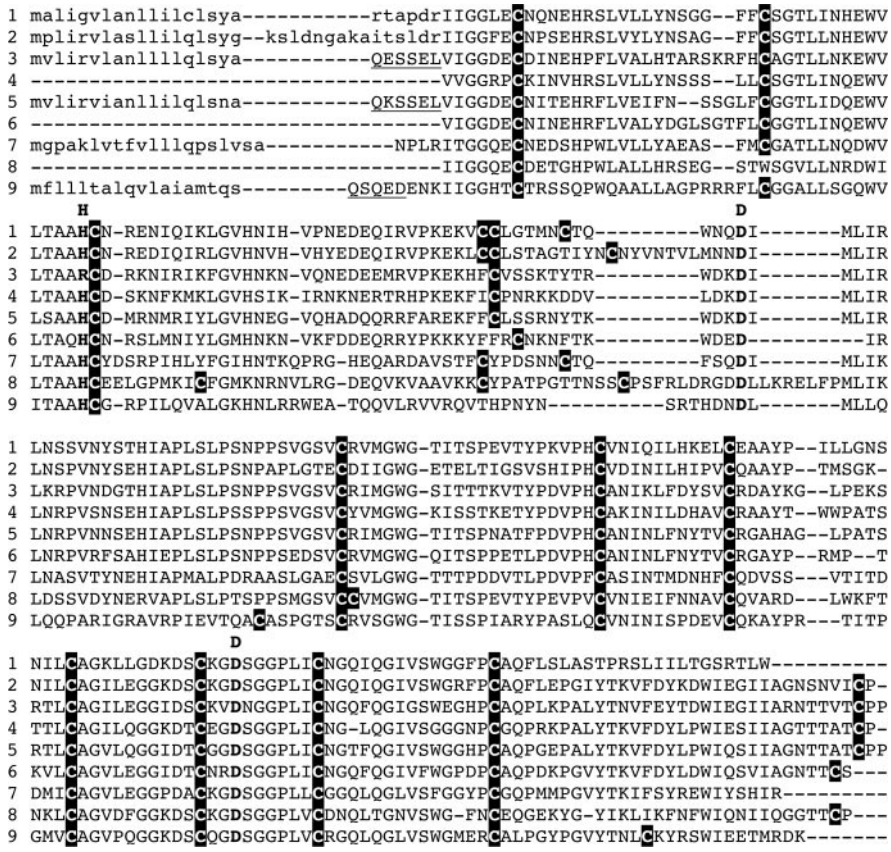

FIG. 8. **Sequence alignment of the representative full-length (unless otherwise indicated) kallikrein toxins.** *1*, partial sequence Q2XXM2 from *P. olfersii*; *2*, Q5MCS0 from *L. curtus*; *3*, Q6T6S7 from *Bitis gabonica*; *4*, P81824; *5*, Q9PTU8, both from *Bothrops jararaca*; *6*, P33589 from *Lachesis muta*; *7*, Q2XXN0 from *V. varius*; *8*, P43685 from *H. horridum*; *9*, the non-toxin representative Q9POG3 from *H. sapiens*.

variable among the non-front-fanged snakes, ranging from solid smooth fangs (type 1) to grooved fangs of varying depth and length (types 2–4) (Table III). Tooth size was also variable with significant enlargement occurring on multiple independent occasions. Particularly enlarged teeth were observed in representatives from all families, such as *Dispholidus* and *Oligodon* in Colubridae, *Tomodon* and *Waglerophis* in Dipsadidae, *Macropisthodon* in Natricidae, *Malpolon* and *Rhamphiophis* in Psammophiinae, and *Homalopsis* in Homalopsidae. In contrast, *Atractaspis* plus all elapids and viperids possessed type 5 dentition with an enclosed venom canal, and relative tooth size was also much less variable.

DISCUSSION

Molecular Characterization of Caenophidia Venoms—Complex venoms are a feature of the well studied elapids, viperids, and *Atractaspis* and have also recently been shown to be a feature of the helodermatid and varanid venomous lizards (4). In this study, multiple toxin types were sequenced from all non-front-fanged snake cDNA libraries, indicating the common presence of complex venom transcriptomes containing multiple bioactive components. For hyaluronidase, kunitz, and waprin these were the first sequences, whether protein or nucleotide, obtained for non-front-fanged species. For 3FTx, CRISP, kallikrein, lectin, MMP, PLA_2, and SVMP/ADAM, only a very few proteins had been previously even partially sequenced from non-front-fanged species. For 3FTx, CRISP, lectin, and kallikrein, taxonomically limited cDNA sequences were previously reported, but comprehensive comparisons had not been undertaken.

In the sequencing surveys undertaken in this study, transcripts of 3FTx, CRISP, and SVMP/ADAM were the most phylogenetically widespread dominantly secreted toxin types, occurring in at least seven of the 10 non-front-fanged snakes examined. Other phylogenetically widespread dominant toxin transcripts were lectin and waprin. Identification of 3FTx transcripts as a common component of caenophidian venom is consistent with previous studies showing active expression of potent 3FTx in a range of non-front-fanged snakes (2, 14, 40). Similarly for the other toxin types, the congruence with previous LC/MS data on the same species provides additional evidence of active expression of bioactive proteins in the venom glands of non-front-fanged snakes (14). Multiple transcripts of the majority of toxins were recovered from individual cDNA libraries; this pattern is consistent with accelerated diversification in toxin multigene families as observed in elapids and viperids (19). Numerous transcripts were recovered with significant variations including changes in key functional residues, changes in the number and spacing of cysteine residues, and large scale deletions. These modifications represent potential neofunctionalization (evolution of novel bioactivities). These results support previous suggestions that

the venom system is a basal characteristic of the advanced snakes (3, 4) and also previous crude venom studies (14, 16, 17). This has important implications for understanding the evolution and ecology of the advanced snake radiation and identifies venoms from non-front-fanged snakes as an important bioresource.

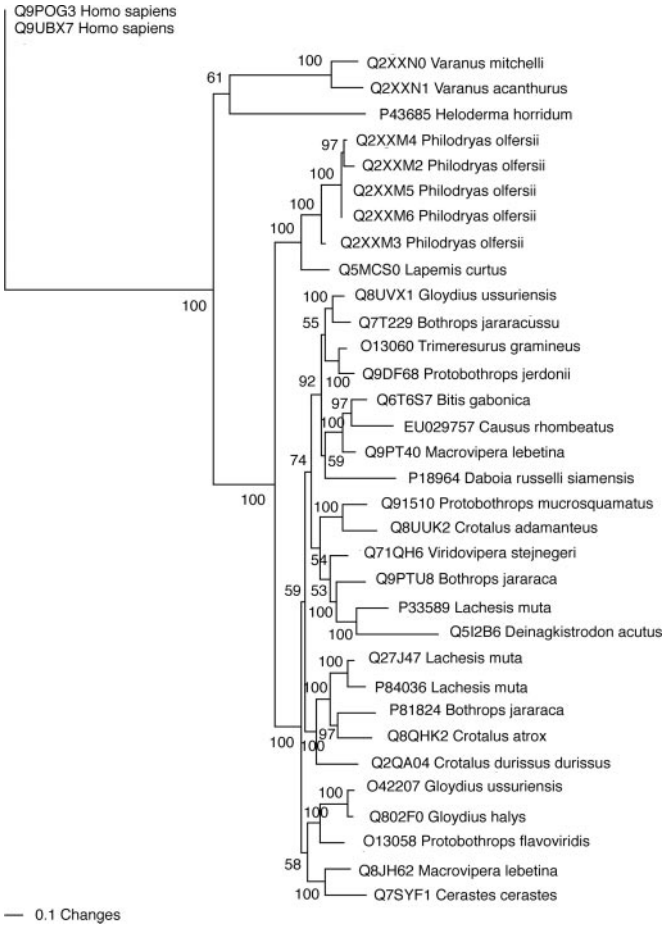

FIG. 9. **Bayesian molecular phylogeny of kallikrein toxins.** Outgroups are non-toxin forms Q9GOG3 and Q9UBX7 from *H. sapiens*.

Despite their relative presence, these toxin types in different lineages should not be considered the only classes present in a particular venom. This caveat is due to the limited sequencing that detected only the major toxin transcripts for each species. Other types may be present at lower expression levels. It is likely that more detailed exploration of their venoms will reveal the presence of additional toxin types. This is demonstrated by this study recovering only 3FTx, CRISP, factor X, kunitz, and Type IB PLA_2 from *O. microlepidotus* but not other toxin types previously sequenced from this species such as factor V, natriuretic peptides, or nerve growth factor.

Toxin Structure-Function Relationships—Structure-function relationships of a number of the toxin types sequenced in this study have been well characterized in venoms from snakes (*Atractaspis*, elapids, or viperids) or helodermatid lizards (Table II) (20). This includes information on the key amino acid residues necessary for conferring toxicity (*e.g.* CRISP proteins (30–35)), the role of cysteine spacing in determining folding structure and toxicity, and a demonstrated role for novel mutations such as large scale deletions in conferring new bioactivities.

CRISP toxin transcripts were present in the majority of the venom glands examined. Previous analysis of CRISP toxin sequences from the venom of the natricid snake *R. tigrinus* showed that it lacked the EX_2F motif thought to be responsible for the smooth muscle paralytic effect as well as the KX_6KR motif hypothesized to be essential for the inhibition of cyclic nucleotide-gated calcium channels. Subsequent bioactivity testing confirmed that *R. tigrinus* CRISP toxin indeed lacked these activities (31, 32, 42, 43), but it was unclear whether this was representative of CRISP toxins from the venoms of other non-front-fanged snakes. In this study, forms containing the EX_2F motif were present in some venoms (Figs. 5 and 6). Translation and expression of these encoded proteins would thus likely induce smooth muscle paralysis. It is notable that CRISP toxins are particularly rich in the venoms of species that are reptilian feeders (14) such as *T. dhara* and *T. biscutatus*. It may be that the toxic hypothermic effect is useful in slowing down the movement of exothermic prey. Studies on this aspect

FIG. 10. **Sequence alignment of kunitz toxins with functional residues (protease-inhibiting reactive bond) shown in *bold* and the leader sequence shown in *lowercase*.** *1*, EU029687 from *T. dhara*; *2*, EU029688 from *P. olfersii*; *3*, P24541 from *Eristocophis macmahonii*; *4*, P82966 from *O. hannah*; *5*, P19859 from *N. naja*; *6*, P00981 from *Dendroaspis polylepis*; *7*, Q7LZE4 from *O. scutellatus*; *8*, Q90WA0 from *P. textilis*; *9*, P00989 from *B. multicinctus*; *10*, the representative non-toxin P04815 from *Bos taurus*.

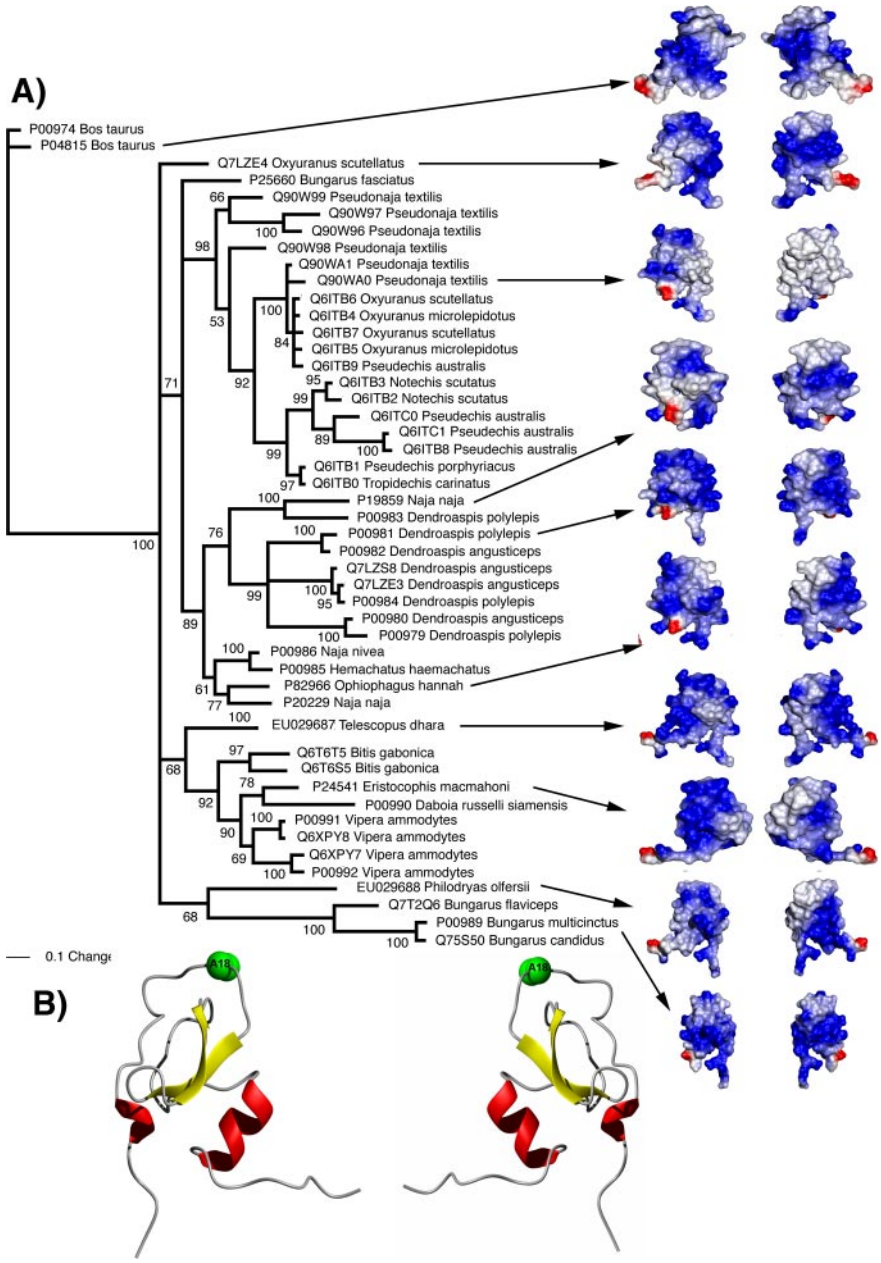

FIG. 11. *A*, Bayesian molecular phylogeny of kunitz toxins. The outgroup is the non-toxin P04815 from *B. taurus*. *B*, ribbon view of EU029687 from *T. dhara*. α-Helices are in *red*, β-strands are in *yellow*, and the functional residue Ala-18 is shown in *green*.

may shed significant light into the evolutionary pressures driving the molecular diversification of this toxin type.

Cation-permeable channels (sodium-, potassium-, and calcium-selective channels as well as cyclic nucleotide-gated channels, which are unselective for monovalent Na^+ and K^+ but also allow transfer of Ca^{2+} cations) often contain more than one binding site for channel blockers, one generally within the transmembrane bundle to bind *e.g.* anesthetics and one or more at their extracellular side that interact with toxins. A most effective channel block occurs when the ion permeation pore is directly occluded by a toxin from the extracellular side. This pore in many cases is bevelled, narrowing toward a selectivity filter (*i.e.* in potassium, calcium, and sodium channels). To attract positively charged ions this pore contains both acidic and aromatic residues. Therefore, extracellular channel blockers often contain positive charges, *i.e.* guanidinium groups as in arginine, which are flanked by H-bond donors, like in conotoxins and dendrotoxins. Due to their size, venom proteins can affect channel gating only from the extracellular side. We postulate that to occlude the channel pore these proteins require a 3D structure motif that (i) is accessible to interact with an ion channel, (ii) consists of one (ideally positively) charged residue to interact with the charged amino acids inside the ion permeation pore, (iii) exhibits one or more H-bond donor(s) in vicinity to the charged residue, and (iv) possibly contains an aromatic

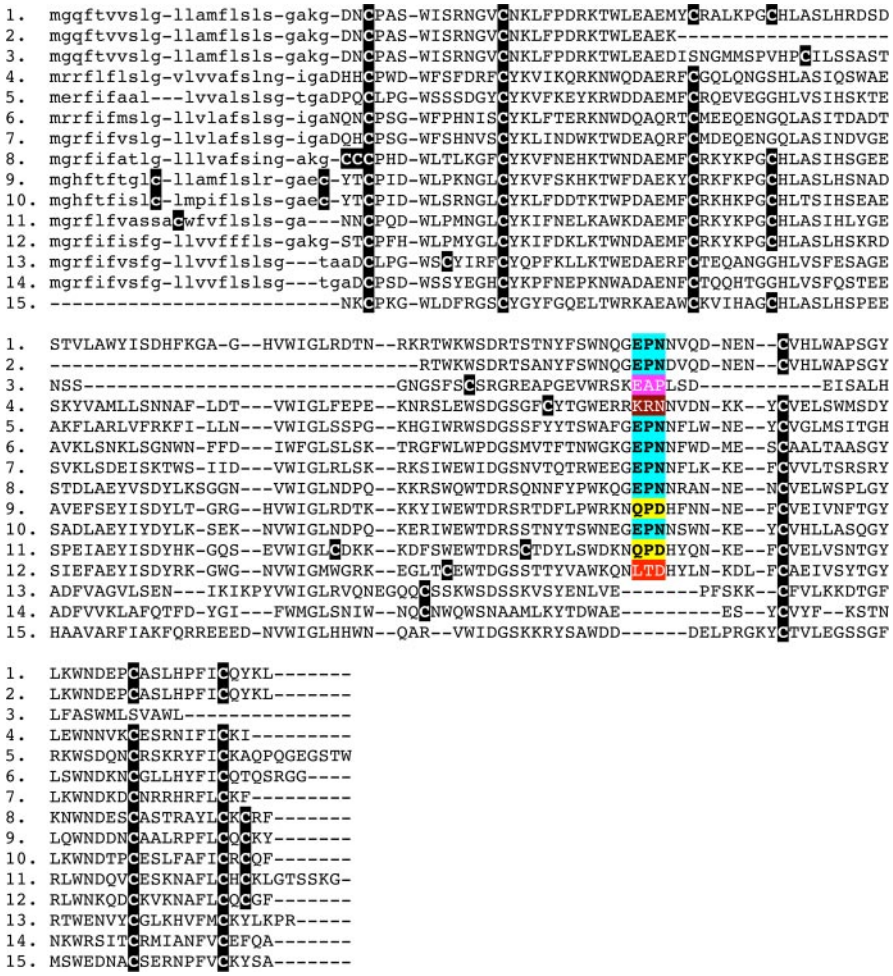

FIG. 12. **Sequence comparison of representative lectin toxins.** The homomeric forms shown are: *1*, EU029691; *2*, EU029689; *3*, EU091713, all from *E. polylepis*; *4*, EU029699 from *L. madagascariensis*; *5*, EU029697; *6*, EU029702, both from *L. poecilogyrus*; *7*, EU029700 from *P. olfersii*; *8*, EU029696 from *T. jacksonii*; *9*, Q90WI6 from *B. multicinctus*; *10*, *Micrurus corallinus* sequence published but not database-curated (62); *11*, Q6TRS6 from *Bothrops jararacussu*; and *12*, Q6T7B7 from *B. gabonica*. Representative heterodimeric forms (α- and β-chains, respectively) shown are: *13*, Q8JIV6; and *14*, Q8JIV7A, both from *D. acutus*. Also included is the representative non-toxin form: *15*, P83300 from *Anser anser*.

amino acid to form either π-π or cation-π interactions with the channel pore.

Structural studies revealed that CRISP is a two-domain protein of conserved fold consisting of a pathogenesis-related PR-1 and a CRD, which are linked together via a flexible hinge (30, 44). Although significantly smaller than PR-1, the CRD spans the C-terminal six of a total of 16 conserved cysteines. The resulting three disulfide bonds stabilize the CRD fold and leave only marginal room for movement in this domain. It is widely assumed that hydrophobic residues of a concave cleft including both the PR-1 and the cysteine-rich domain would bind the CRISP to the ion channel (30), whereas actual channel block is hypothesized to involve amino acids of CRD only. The fact that CRISP toxins block a variety of ion channels may indicate that different residues located at different positions of CRD are responsible for occluding the extracellular entry to the channel. This hypothesis is supported by the observation that CRD can move relative to the PR-1 domain, which may even lead to exposure of residues that in the experimental x-ray structures (Protein Data Bank codes 1RC9 (44) and 1XX5 (31)) are found at the interface to PR-1. Yet the amino acids actually blocking ion channels remained unidentified to date and were mainly postulated from multiple sequence alignments. To our understanding, the cysteine-rich domain contains three sites, which may putatively block ion channels: (i) the loop between β11 and α7 spanning eight residues between the first and second cysteine in CRD, (ii) the loop connecting α7 and α8 containing up to six amino acids, and (iii) the C-terminal tail following the sixth conserved CRD cysteine.

A hypothesized functional EX_2F motif (34, 35) was found three to six residues C-terminal to the first CRD cysteine. In this study we could not confirm this motif to be conserved and thus functional throughout the CRISP family. However, the widespread taxonomical presence is suggestive that if this motif is not basal it is at least early emerging. Whereas the aromatic residue was conserved (either phenylalanine or tyrosine), the glutamate occurred in only five of 16 sequences. At the same position five asparagines, one glutamine, and two lysines were found, but interestingly no aspartate was found. In contrast, the C-terminal neighbor to glutamate in position +3 of the first CRD cysteine is highly conserved exhibiting only aspartate (nine occurrences) and asparagine (11 occurrences). This position corresponds to the first residue in the DVF motif that has been identified to selectively interact with

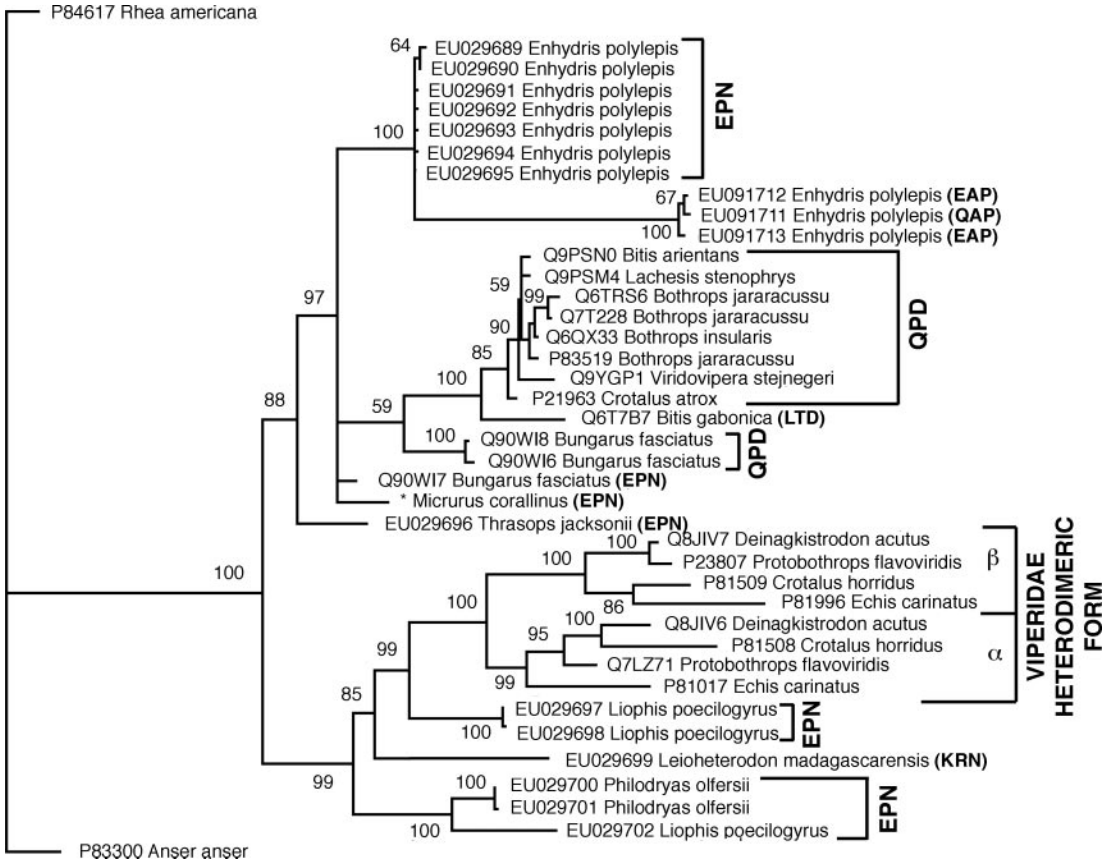

FIG. 13. **Bayesian molecular phylogeny of lectin toxins.** The outgroup is the non-toxin P83300 from *A. anser*. *, *M. corallinus* sequence published but not database-curated (62).

L-type calcium channels (35). It ranges from position 4 to 6 after the first CRD cysteine. This motif was first identified in ω-conotoxin TxVII (45) and was later found in the venom protein ablomin (35). Our structural studies showed that the side chain of the aspartate/asparagine in DVF was oriented toward the core of CRD forming several H-bonds with the third and most C-terminal a-helix α9. The second and third residues of this motif are located at the surface of CRD with their side chains pointing toward the solvent. Yet valine was found only three times in this study, whereas in 14 instances this residue was charged (four times lysine and 10 times glutamate and aspartate). The third residue of this motif was large and hydrophobic and, with the exception of the sequence Q3SB05 from *Pseudonaja textilis*, aromatic. We hypothesize that these two residues may dock to ion channels because they satisfy, in most cases, the four criteria postulated earlier: (i) spatial accessibility, (ii) a charged amino acid, (iii) nearby H-bond donors, and (iv) an aromatic residue in spatial proximity to the charged amino acid. Exceptions to criterion ii are several hydrophobic or polar residues found in *D. typus*, *L. poecilogyrus*, *E. polylepis*, *Lapemis curtus*, *Protobothrops mucrosquamatus*, and *Heloderma horridum*. Interestingly potential H-bond donors are available in positions −1 and −2 of the fourth CRD cysteine (Fig. 5).

Alternatively, interactions with L-type calcium channels may involve one of the following motifs. (i) The loop tip between helices α7 and α8 may be involved. Here the first residue of the loop is either polar (Gln or Asn) or charged (Lys or Glu) followed by a mostly polar (Asn, Ser, or Thr) and an either polar (Ser, Asn, Thr, or His) or charged amino acid (Lys or Asp) just before the third conserved cysteine. This region contains charged residues in many toxins and is structurally exposed. However, it lacks an aromatic amino acid in its vicinity. (ii) The residues in position +1 or +2 of the first and in +1 of the fifth conserved CRD cysteine may be involved. The former was postulated to be involved in cyclic nucleotide-gated channel block and often contains a basic amino acid (see below and Fig. 5); the latter is predominantly phenylalanine. This substructure is also accessible and is held in place by a nearby disulfide bond. (iii) Positions +1, +2, and +3 after the sixth CRD cysteine may be involved. This part of the C terminus is mostly positively charged and polar. It is relatively flexible and accessible and may therefore interact with L-type calcium channels.

Morita and co-workers (32, 33, 35) proposed one or two residues immediately C-terminal of the first conserved CRD cysteine to be critical for interaction with cyclic nucleotide-gated ion channels. Their work revealed that the C-terminal

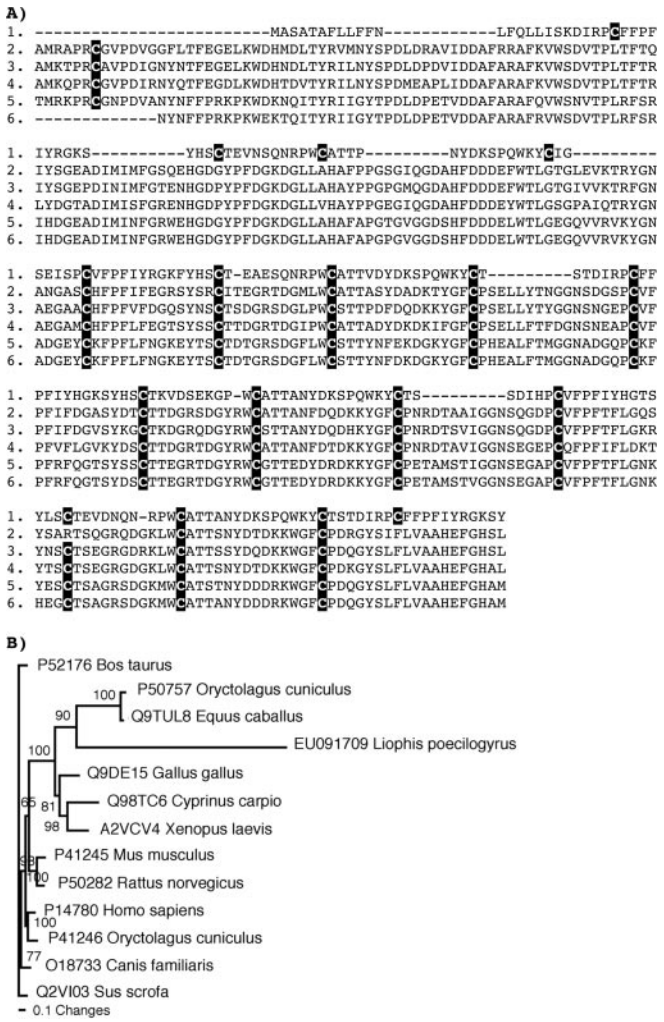

FIG. 14. **Matrix metalloprotease.** *A*, partial sequence alignment of EU091709 from *L. poecilogyrus* (*1*), Q9DE15 from *G. gallus* (*2*), A2VCV4 from *X. laevis* (*3*), Q98TC6 from *Cyprinus carpio* (*4*), P50757 from *Oryctolagus cuniculus* (*5*), and Q9TUL8 from *Equus caballus* (*6*). *B*, Bayesian molecular phylogeny of lectin toxins. The outgroup is the non-toxin P52176 from *B. taurus.*

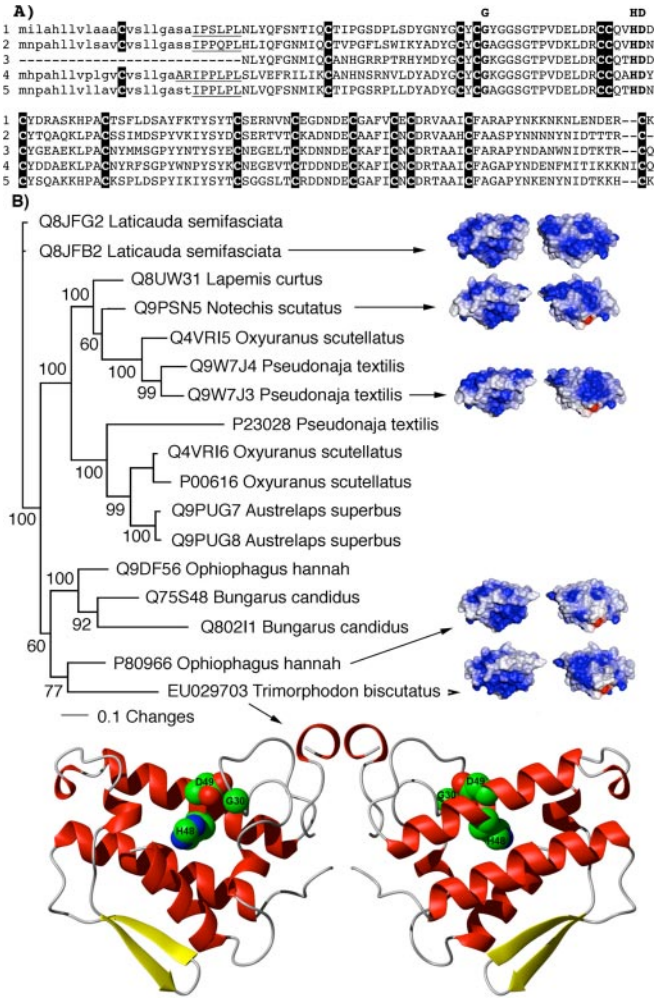

FIG. 15. **PLA_2 (Type IB) analyses.** *A*, sequence alignment of representative toxins. *1*, EU029703 from *T. biscutatus*; *2*, P80966 from *O. hannah*; *3*, Q9PSN5 from *Notechis scutatus*; *4*, Q9W7J3 from *P. textilis*; *5*, the non-toxin representative Q8JFB2 from *L. semifasciata* pancreas. *B*, Bayesian molecular phylogeny; the outgroup is Q8JFB2 from *L. semifasciata* liver. The ribbon model of TRI002F09 from *T. biscutatus* shows the conserved catalytic residues (63). α-Helices are in *red*, and β-strands are in *yellow*.

domains of pseudechetoxin and pseudecin, which are very similar to CRD, were identical but for two residues. The KR motif in pseudechetoxin made this protein more susceptible to cyclic nucleotide-gated block than the NY of pseudecin. In this work, seven of 19 specimens had a positively charged residue in either position +1 or +2 of the first cysteine (Fig. 5). For these specimens, we therefore postulate some activity to block cyclic nucleotide-gated channels.

Modification of structural residues was also evident in numerous caenophidian venom toxin transcripts. It has been shown that changes in the spacing of ancestral cysteines, the occurrence of newly evolved cysteines, and modifications in structural residues flanking the cysteines can alter the three-dimensional structure of the molecule and thus the residues contributing to the surface chemistry with consequences for bioactivity (20). Such modifications can produce toxin variants that have specificities or potencies differing radically from previously characterized forms, including the potential emergence of neofunctionalizations.

Most of the 3FTxs sequenced in this study retained the ancestral 10-cysteine arrangement (19) (Fig. 2) as had been shown previously for the α-neurotoxic 3FTx from the venom of the colubrid *C. radiatus* (2). However, the conservation of the ancestral cysteines does not preclude bioactivities other than α-neurotoxicity as typified by a form from the venom of the colubrid snake *Boiga dendrophila* that retained the ancestral cysteines yet was only weakly α-neurotoxic but had a newly derived presynaptic mode of neurotoxicity (16). As the sequences obtained in this study were even more divergent, including the evolution of alternate cysteines, it is quite likely that a multiplicity of novel activities has been derived.

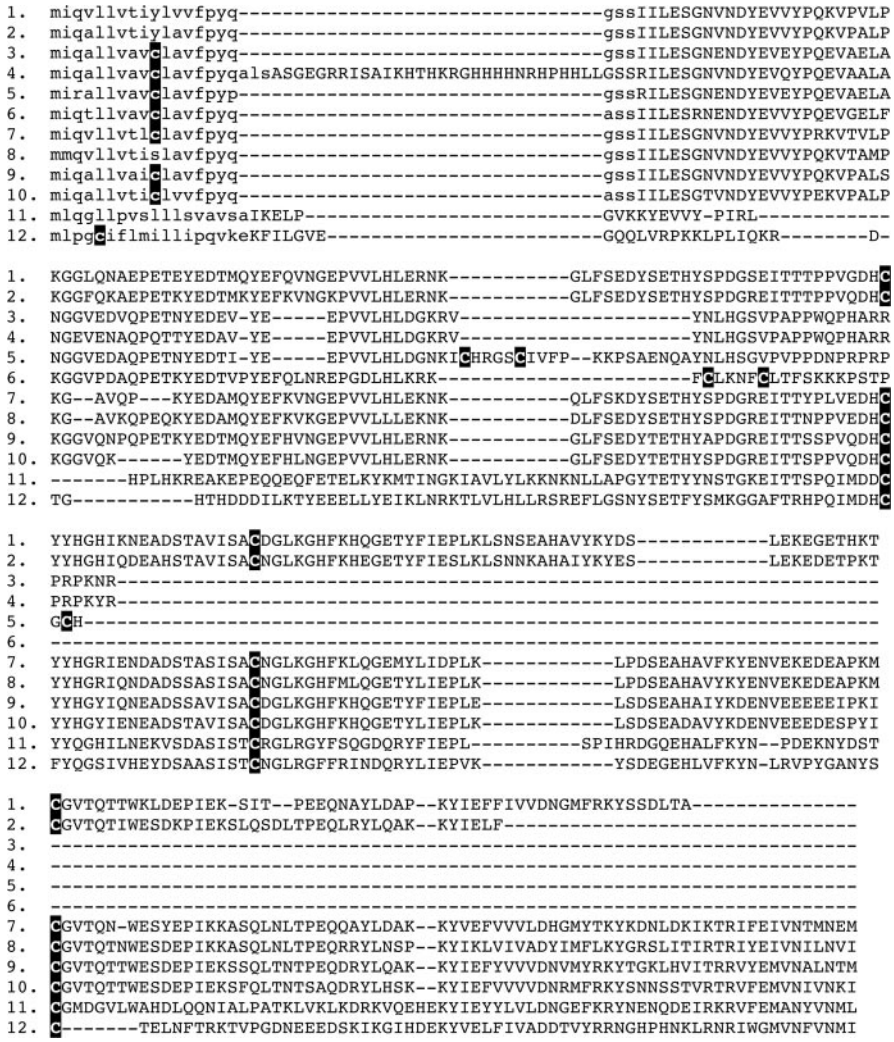

FIG. 16. **N-terminal sequence alignment of SVMP/ADAM toxins.** The partial sequences from non-front-fanged advanced snakes are: *1*, EU029705 from *P. olfersii*; and *2*, EU029707 from *L. poecilogyrus*. The full-length unique truncated forms are: *3*, EU029708; *4*, EU029713; *5*, EU029717; and *6*, EU029727, all from *P. mossambicus*. The representative viperid venom sequences are: *7*, O42138 from *Agkistrodon contortrix laticinctus*; and *8*, Q4VM08 from *Macrovipera lebetina*. *9*, the representative elapid sequence Q8JGN1 from *Naja mossambica*. *10*, the representative atractaspidid venom form Q9PT48 from *A. engaddensis*. The representative non-toxin forms are: *11*, Q9UKQ2 (ADAM28 type); and *12*, Q9H2U9 (ADAM7 type) from *H. sapiens.*

In addition to variations in functional residues and cysteines, mutants were also sequenced with frameshifts, truncations, and putative exon deletions. Novel transcripts of the SVMP/ADAM toxin type were isolated from *P. mossambicus* that were comprised solely of the propeptide domain (Fig. 16). Although forms of SVMP/ADAM have been identified previously that selectively express a particular domain (*e.g.* comprised solely of the disintegrin domain (19)) this is the first time that the prepro domain has been discovered as being selectively expressed as the sole domain. The putative exon deletion in the lectin toxin variant from *E. polylepis* not only removed a large stretch of residues but also one of the ancestral cysteines, leaving a free cysteine, potentially facilitating dimerization (Fig. 12). Similarly the putative frameshift in the lectin toxin variant from *E. polylepis* produced transcripts with even numbers of cysteines, and therefore these sequences may be able to fold to produce stable frameworks (Fig. 12). Thus, genomic mutations in both the caenophidian SVMP/ADAM and lectin toxins have the potential to produce functional proteins with significantly altered bioactivities.

Venom toxins from non-front-fanged snakes may also prove useful for investigations of the structure-function relationships of the normal body proteins from which they were derived (20). In some cases, much more is known about the toxic forms than the ancestral body homologues. For example, the normal body forms of the CRISP proteins are poorly characterized with virtually nothing known of their bioactivities. Even the activities of forms that may play important roles, such as those with high expression levels in specific tissue or organs, remain unknown. The basal activity of the CRISP venom protein is likely to be relaxation of peripheral smooth muscle, such as helothermine from *H. horridum* (46), and may indicate a tissue-specific role for the ancestral normal body protein. The kallikrein toxins are an example of where an ancestral body action (liberation of bradykinin from kininogen) is preserved, but some toxin isoforms have derived additional activities (*e.g.* cleavage of fibrinogen). Similarly the two independently recruited types of PLA_2 proteins in snake venoms have derived activities that the normal body form lacks (*e.g.* antiplatelet toxicity, myotoxicity, and neurotoxicity). Consist-

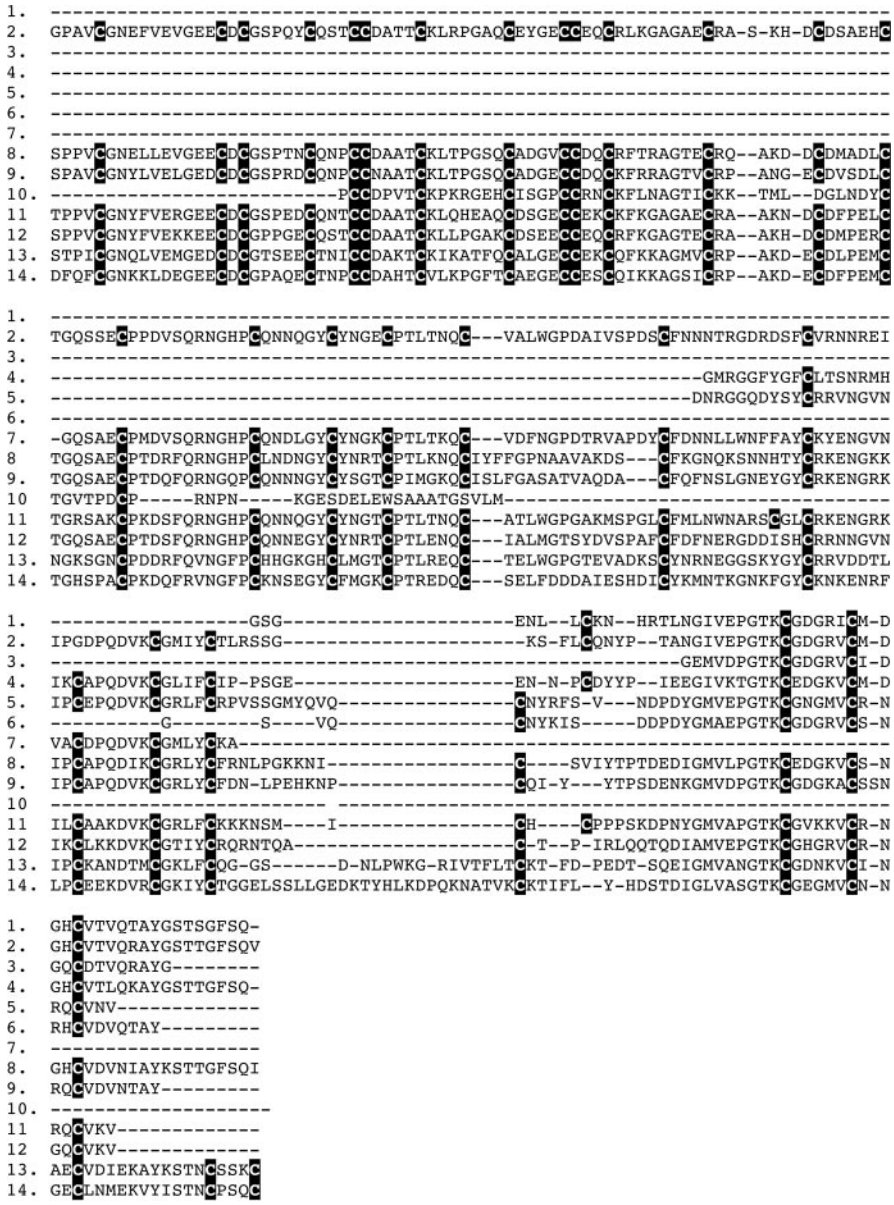

FIG. 17. **C-terminal sequence alignment of SVMP/ADAM toxins.** The partial sequences from non-front-fanged snakes are: *1*, EU029734; *2*, EU029736; *3*, EU029737, all from *D. typus*; *4*, EU029735 from *T. jacksonii*; *5*, EU029738; *6*, EU029739, both from *L. madagascariensis*; and *7*, EU036637 from *T. dhara*. The typical viperid venom forms are: *8*, O42138 from *A. contortrix laticinctus*; and 9, Q4VM08 from *M. lebetina*. *10*, the representative truncated disintegrin form Q6T6T2 from *B. gabonica*. *11*, the representative elapid sequence Q8JGN1 from *N. mossambica*. *12*, the representative atractaspidid venom form Q9PT48 from *A. engaddensis*. The representative non-toxin forms are: *13*, Q9UKQ2 (ADAM28 representative); and *14*, Q9H2U9 (ADAM7 representative) from *H. sapiens.*

ent with this, the toxic forms contain a positively charged hotspot on the surface that is lacking in the ancestral form from the pancreas (Fig. 15). The venom proteins therefore represent exquisite natural "knock-out" studies of tremendous usefulness in elucidating the structure-function relationships of the non-toxin, body homologues of physiological importance. The relative assignment of conserved/variable functional residues should not be considered definitive as not all sites/proteins are well characterized, and other transcripts/toxin types may contain functional residues that confer ancestral or novel bioactivities, especially for the toxin types not listed above.

Timing of Toxin Recruitment Events—The phylogenetic distribution of venom toxins in the Toxicofera (venomous squamates) provides insights into the timing of toxin recruitment events (Fig. 1). The majority of snake venom toxins (14 of 27) are either shared with the two other Toxicofera lineages (Iguania and Anguimorpha) (7 of 27) or occur near the base of the Caenophidia snake clade (7 of 27). The independent evolutions of advanced front-fang architectures in *Atractaspis* and Viperidae are linked with recruitments of new toxin types (Fig. 1). In the viperids, two new toxin types, c-type natriuretic peptide-bradykinin-potentiating peptide and PLA_2 (Type IIA), are closely linked to the evolution of advanced venom delivery systems and ambush feeding, whereas four other toxin types were evolved later on (renin-like aspartic protease, cytokine FAM3B, glycine-rich toxin, and waglerin). The evolution of advanced venom architecture in viperids also coincides with significant molecular diversification of two existing toxin types (SVMP/ADAM and kallikrein). The evolution of sarafotoxins in *Atractaspis* is also closely timed with the evolution of ad-

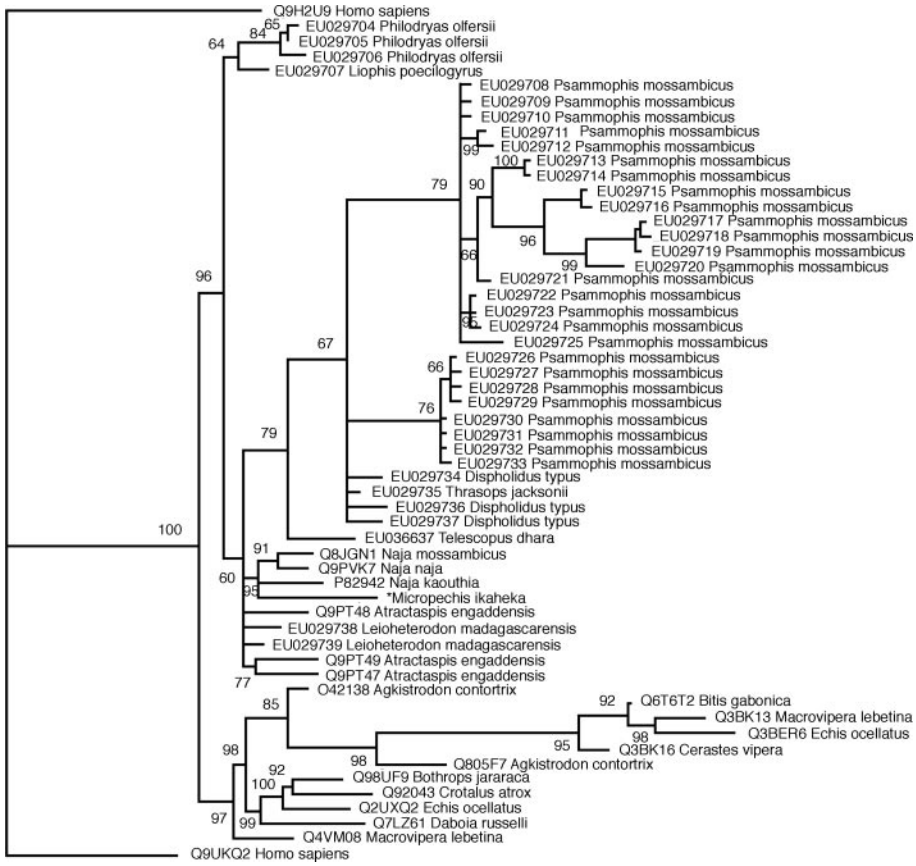

FIG. 18. **Bayesian molecular phylogeny of SVMP/ADAM toxins.** The outgroup is the non-toxin ADAM28 sequence Q9UKQ2 from *H. sapiens*. *, a published but uncurated sequence from *Micropechis ikaheka* (64).

vanced front fangs, but whether as a cause or an effect (occurring before or after) the evolution of hollow fangs remains to be elucidated. In the elapids, the only two additional toxin types currently known do not coincide with development of a high pressure front-fanged venom system with the hole-punching, short stubby fangs useful for penetrating tough reptile scales. Instead the evolution of new venom systems appears to also be linked to the explosive diversification of existing toxin types: 3FTx and PLA_2 (Type IB) toxins in the elapids with numerous new bioactivities developed for each toxin type. The only documented newly evolved toxin types are found within the rapidly radiated Australian elapid snakes. One evolved at the base of this clade (factor X), and one evolved in the common ancestor of *Pseudonaja* and *Oxyuranus* (factor V).

The very long, derived glands of *C. rhombeatus* do not appear to be linked to the evolution of new toxin types either with the dominant toxin types being CRISP, kallikrein, Type IIA PLA_2, and SVMP/ADAM (including RGD disintegrins). Within *Atractaspis* the venom differences between long and short glanded species is unclear. It is also unknown whether the long glands of some *Calliophis* species are linked to significant changes in venom composition.

The early recruitment of a LYNX/SLUR-like gene to form the 3FTx toxin multigene family was one of the most significant developments in snake venom evolution, priming the Caenophidia for extensive diversification. Indeed, venoms from non-front-fanged species have been shown to be just as toxic as well characterized extremely potent elapid venoms (40). A unique nuance of this potent and fast acting toxin type is that, unlike most other toxins, the lethality is almost the same whether injected subcutaneously, intramuscularly, or even intravenously (19), and therefore delivery just under the skin is as efficient as straight into the bloodstream. The highest expression levels of this toxin type in the non-front-fanged snake families are in the gracile, fast moving forms that have only slightly or moderately enlarged rear maxillary teeth and predate upon fast moving, soft, thin skinned, non-dangerous prey items such as geckos and frogs (14). In contrast, the long fanged *D. typus* is an arboreal snake that includes birds as a major prey item, and the venom is rich in forms of the SVMP/ADAM toxins that are potently prothrombin-activating. The fish-eating aquatic homalopsid snakes, which also have large maxillary dentition, favor hemotoxic lectin toxins as well as ADAM toxins. The elapid snakes, which puncture tough reptile skin with their short, strong hollow front fangs, also typically express 3FTx transcripts as the dominant mRNA species. However, they favor the derived forms that lack the second and third ancestral cysteines.

Within the elapids additional toxin types were evolved later on but also with tremendous impact, such as factor X at the base of the Australian elapid clade and factor V in the common ancestor of *Pseudonaja*/*Oxyuranus*. The recruitment of

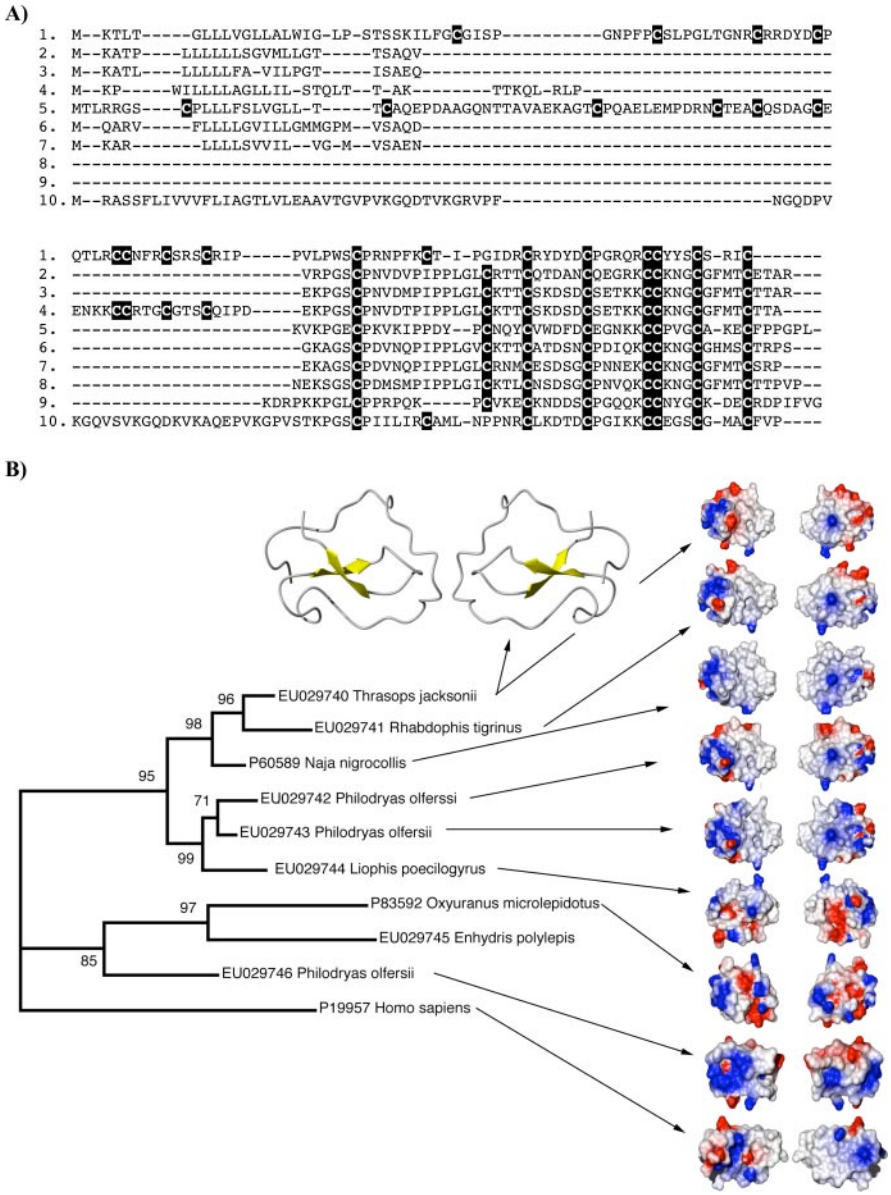

FIG. 19. *A*, sequence comparison of representative waprin toxins from non-front-fanged advanced snakes (*1*, EU029745 from *E. polylepis*; *2*, EU029744 from *L. poecilogyrus*; *3*, EU029743; *4*, EU029746; *5*, EU029742, all from *P. olfersii*; *6*, EU029741 from *R. tigrinus*; *7*, EU029740 from *T. jacksonii*) and from front-fanged advanced snakes (*8*, P60589 from *Naja nigricollis*; *9*, P83952 from *O. microlepidotus*) and of the representative non-toxin form (*10*, P19957 from *H. sapiens*). *B*, Bayesian molecular phylogeny of waprin toxins. The outgroup is the non-toxin P83300 from *A. anser*. The ribbon model of EU029740 from *T. jacksonii* shows β-strands in *yellow*.

factor X and factor V in the Australian clade of elapids would have also tremendously aided prey capture with only a small amount of these very active enzymes needed to cause severe disruption of blood chemistry. However, the activity of factor X toxins is rate-limited by the requirement for cofactors, particularly the essential need to form a 1:1 complex with factor V (47). Thus, the recruitment of factor V into the venom of the *Oxyuranus*/*Pseudonaja* clade resulted in a virtually complete, perfect toxin complex, greatly increasing the relative toxicity of the venoms and thus significantly aiding in the prey capturing ability. Subsequent to the recruitment of factor V, the *Oxyuranus*/*Pseudonaja* common ancestor split into two very different forms despite the two genera remaining very closely genetically related.

The *Oxyuranus* species are very large snakes with extremely long fangs and high venom yields. Unlike most Australian snakes, which often feed on reptiles, these snakes feed exclusively on mammalian prey including large rats and bandicoots, dangerous prey items capable of an adept defense potentially causing serious injury to the snake predators. The snakes successfully feed on such dangerous prey by minimizing prey contact time through the use of a snap-release form of striking along with a tendency for multiple strikes, thus overwhelming the prey items with copious amounts of the extraordinarily potent venom delivered deep into the tissues several times. A limitation of this form of prey capture is that the snakes need to be very warm to successfully use this energetically costly form of prey capture. Consequently their habitat is limited only to the tropical north of Australia and in New Guinea (*Oxyuranus scutellatus*) and the

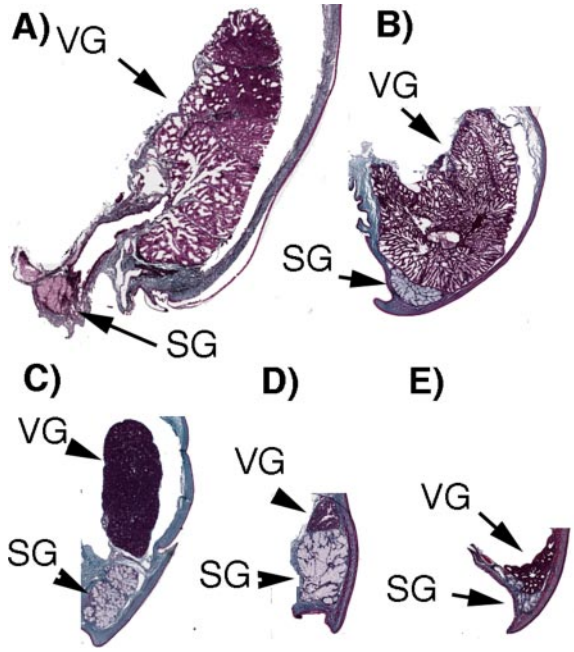

FIG. 20. **Transverse histology of Masson's trichrome-stained sections showing the relative size of venom glands (proportional to head size) for *H. leopardinus* (*A*), *D. typus* (*B*), *Homalopsis buccata* (*C*), *P. guttatus* (*D*), and *D. scabra* (*E*).** *VG*, venom gland; *SG*, supralabial gland.

baking heat of the channel country in the Australian outback (*O. microlepidotus*).

In contrast, the *Pseudonaja* species have taken a very different evolutionary path, taking advantage of possessing such toxic venom to greatly minimize the amount of biological energy expended in venom production. *Pseudonaja* species are smaller snakes with very short fangs and much smaller venom yields, utilizing constriction to hold non-dangerous prey items (such as reptiles) in place while envenomating. As these snakes do not expend as much energy in prey capture, they do not have to be as warmed up as the *Oxyuranus* species. These snakes consequently have taken advantage of their extremely toxic venom to become one of the most adaptable and successful snake types of the entire Australian continent.

Another conspicuous finding of this study was the resolution of the lectin toxins into a single clade with homomeric forms not reciprocally monophyletic in relation to the heterodimeric form found exclusively in viperid venoms (Fig. 13). The homomeric and the heterodimeric lectin forms had been considered previously to be the result of two separate toxin recruitment events (3) or the result of a single recruitment event (18). However, reconstructing the evolutionary history had been hampered by the scarcity of homomeric sequences.

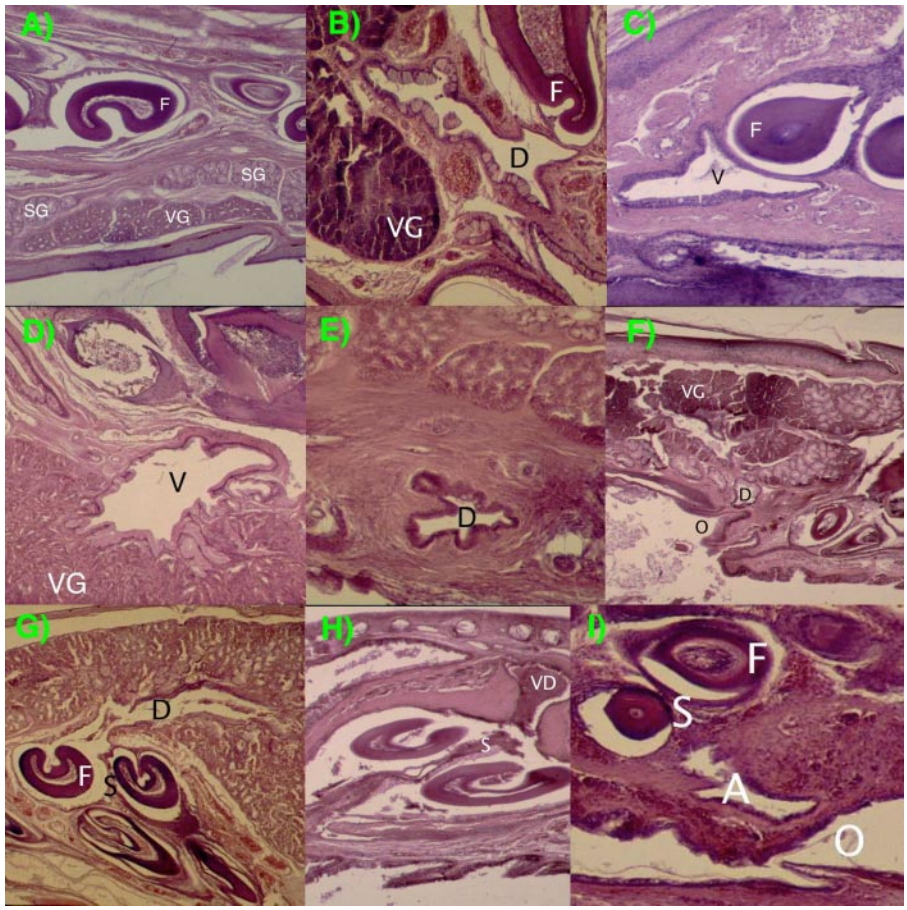

FIG. 21. **Histology using modified Van Gieson's stain.** *A*, frontal section through *Ahaetulla nasuta* showing the structural differences between the supralabial gland and venom gland. *B*, transverse section showing a proximal to distal transition in the epithelial lining of the venom duct of *Psammophis schokari*. *C*, frontal section showing the relatively small venom vestibule of *D. punctatus* located adjacent to the fang. *D*, frontal section through *R. tigrinus* showing the venom vestibule located immediately adjacent to the venom gland. *E*, frontal section through the venom duct of *T. capensis* showing the concentric rings of surrounding connective tissue. *F*, transverse section through the venom duct of *Coluber constrictor* showing the venom duct opening to the oral cavity. *G*, frontal section through *Psammodynastes pulverulentus* showing the direct course of the venom duct from the venom gland to the fang sheath. *H*, frontal section through the fang sheath and diverticulum of *Malpolon monspessulanus*. *I*, frontal section through *Oligodon smithii*. showing the accessory venom duct extending away from the fang sheath. *D*, venom duct; *F*, fang; *O*, oral cavity; *S*, fang sheath; *SG*, supralabial gland; *VG*, venom gland; *V*, venom vestibule.

TABLE III
Summary of venom dentition variation in genera studied (for full species list see "Appendix III")

Smooth surface and no enclosed venom canal	Colubridae: *Coluber*, *Dasypeltis*, *Lycodon*, *Masticophis*, *Oligodon*, *Pituophis*, *Philothamnus*, *Spalerosophis*. Dipsadidae: *Diadophis*, *Heterodon*, *Hydrodynastes*, *Hypsiglena*. Lamprophiinae: *Lamprophis*, *Lycophidion*. Natricidae: *Macropisthodon*, *Nerodia*, *Rhabdophis*.
No enclosed venom canal and surface with shallow furrow	Dipsadidae: *Erythrolamprus*. Natricidae: *Amphiesma*.
Deep groove present but restricted to less than half the length of the tooth	Colubridae: *Ahaetulla*, *Chrysopelea*, *Dispholidus*, *Trimorphodon*. Dipsadidae: *Coniophanes*, *Leptodeira*, *Oxyrhopus*, *Pseudoboa*, *Tachymenis*, *Tomodon*. Homalopsidae: *Cerberus*, *Enhydris*, *Erpeton*. Lamprophiinae: *Psammodynastes*. Psammophiinae: *Psammophis*. Pseudoxyrhophiinae: *Madagascarophis*.
Deep groove running the majority of the length of the tooth	Atractaspidinae: *Amblyodipsas*, *Aparallactus*. Colubridae: *Boiga*, *Chionactis*, *Crotaphopeltis*, *Oxybelis*, *Stenorrhina*, *Thelotornis*. Dipsadidae: *Philodryas*. Psammophiinae: *Malpolon*, *Psammophylax*.
Enclosed venom canal	Atractaspidinae: *Atractaspis* only. Elapidae: ubiquitous. Viperidae: ubiquitous.

In this study, we sequenced numerous lectin toxin transcripts from four additional non-front-fanged snake families. This allowed for a more robust reconstruction of the molecular evolutionary history and thus the confirmation that all forms of the snake venom lectin toxins are the result of a single toxin recruitment event (Fig. 1) and that the viperid venom heterodimeric forms arose from within the homomeric basal form (Fig. 13). This study also allowed for the inference that the EPN mannose-binding motif is basal whereas the QPD galactose-binding variant was an early emerging derivation that predated the viperid radiation.

Derivations of the Venom System—Taub (7) described extensive morphological variation within the venom gland (his "Duvernoy's" gland) of non-front-fanged snakes. The present study demonstrates that similar morphological variation exists in the venom duct as well as in the topographic relationship between the venom duct and the fang sheath (see "Appendix I"). These morphological variations do not assort along established evolutionary lines, nor do they correlate well with the attributes of the venoms detailed in this study. This is in contrast to the front-fanged Elapidae and Viperidae families, which each have a well defined, characteristic venom apparatus at the familial level with some minor variations (Fig. 1), such as the size of venom glands and connections of the compressor and other head muscles. The same is true for the front-fanged genus *Atractaspis* but not for the non-front-fanged snakes now included in the Atractaspidinae subfamily, which were shown in this study to be quite variable.

The mechanics of venom injection in front-fanged snakes relies on pressurization of the venom delivery system (48–51). The colubrid snake *D. typus* is the only species with well characterized rudimentary compressor musculature (52), although there is evidence that this has been convergently evolved in the lamprophiine snake *Mehelya capensis* (52) and in the non-front-fanged atractaspidine *Brachyophis revoili* (53). The general absence of these features from the venom delivery system of non-front-fanged snakes suggests that a substantially different mechanism(s) is present within this group. The limited skeletal muscle contact with the venom gland in non-front-fanged snakes (54), the relatively weak wall of the venom duct, and the presence of a venom vestibule would all oppose the pressurization of the venom delivery system (but see Jansen and Foehring (55)). The multiple topographic relationships between the venom duct and the fang, including taxa in which the venom duct opens to the roof of the mouth rather than the fang sheath, clearly indicate that deformation of the fang sheath need not be an important part of venom delivery in non-front-fanged snakes.

Interestingly the colubrid family also contained a clade in which the venom gland was greatly atrophied, the American "rat snake" clade of colubrid snakes, as typified by *P. guttatus* (Figs. 1 and 20). The American rat snakes have secondarily evolved a new form of prey capture (powerful constriction) and prey preference (rodents). Subsequently the gland has become greatly atrophied. Similarly the African *D. scabra*, which feeds exclusively on bird eggs, also has greatly atrophied venom glands (Fig. 20). This is paralleled in the sea snake *Aipysurus eydouxii* that, subsequent to switching from feeding on fish to feeding exclusively on fish eggs, has greatly atrophied venom glands (Fig. 1) and almost entirely lost fangs accompanied by significant accumulation of deleterious mutations to the toxins still transcribed (56, 57). Similarly the lizard egg-eating *Brachyurophis* species of Australian terrestrial elapids also have significant reduction of the venom system. Finally the other few lineages displaying an absence or reduction of the glands are malacophagous (Asian pareatids and some American dipsadids) (1).

Changes in gland size were not restricted to atrophying but also included spectacular lengthening. In each of the front-fanged clades, tremendous elongation has occurred independently: *Atractaspis engaddensis*, *Atractaspis microlepidota*, *Atractaspis micropholis*, and *Atractaspis scortecci* in the Atractaspinae, *Calliophis intestinalis* and *Calliophis bivirgata* in the Elapidae, and *Causus resimus* and *C. rhombeatus* in the Viperidae. The elongations extend to a quarter of the body length. The biological advantage gained by these elongations remains to be elucidated. In at least the case of *Causus* the change in gland length was not accompanied by a significant

shift in venom profile or recruitment of new toxin types. Instead, having typical viperid venom composition with the major toxin types sequenced (SVMP, kallikrein, and PLA_2 (Type IIA)) in this study being consistent with molecular weights obtained in a previous LC/MS study by us (14). It remains to be investigated whether there are significant venom compositional differences between long and short glanded forms within the *Atractaspis* and *Calliophis* genera.

Snakes of Potential Medical Concern—This study has important implications in regard to human medicine by providing new information regarding snake venom composition and thus potential clinical effects of envenomation. It also highlights the potential danger of snakes regarded as of trivial concern based solely upon the lack of severe bites, but in some cases the rarity of reports is due to the rarity of the snake in captivity or encounters in the wild.

This study has shown that the venom transcriptome of *Thrasops jacksonii* is very similar to the extremely potent venom of the very closely related (and proven lethal) *D. typus*, particularly the abundance of PIII-type SVMP/ADAM toxins. The lethality of *D. typus* venom is the result of high expression levels of a potent prothrombin-activating form of the SVMP/ADAM toxin type. In the clinical pathology, the prothrombin activation causes consumptive coagulopathy, resulting in the disappearance of fibrinogen from the blood and the elevated presence of d-dimer products with the ultimate net result of incoagulable blood. Predation by *T. jacksonii* on live mammalian prey results in rapid death in a manner identical to that produced by *D. typus*: profound disruption of hemostasis manifested by rapid and copious bleeding from the mouth and nostrils.[4] Clearly potent venom toxins are actively expressed in this species. We advise exotic animal keepers to treat this species with the utmost caution until studies of the action of *T. jacksonii* venom upon the hemostatic system are undertaken, including the relative neutralization by *D. typus* antivenom. In at least this case, absence of evidence should not be taken as evidence of absence.

Conclusion—Collectively these findings strongly support that there has been extensive evolutionary modification of the venom system in the advanced snake radiation (Caenophidia). All variables appear to change independently ranging from the biochemical variation and specialization of the venoms to the dentition and glandular morphology. The long evolutionary history of the advanced snake radiation (~100 million years) has resulted in extensive diversification of the venom system and shows how little we really know about venom macroevolution and the potential role in the ecology/evolution of the animals themselves. Furthermore the toxin types identified here should not be regarded as the only toxins present in those venoms. Additional experimental efforts will certainly reveal new isoforms of these toxins, and some classes will almost certainly be confirmed as evolving earlier than currently appreciated. Further entirely new toxin types may yet be discovered in any one of the poorly studied snake lineages. Our major findings are of a multidisciplinary nature with uses ranging from evolutionary biology to protein evolution and highlight the underutilization of snake venoms as bioresources in drug design and development.

Acknowledgments—The Naturalis Museum, Leiden, The Netherlands generously loaned us preserved specimens for some of magnetic resonance imaging studies. H. S. is grateful to GlaxoSmithKline for an exclusive version of SPDBV. We are deeply grateful to Professor Elazar Kochva for patience in answering our many questions and for very helpful comments on the manuscript. We also thank the various wildlife departments for the issuing of the relevant scientific collecting permits.

[4] B. G. Fry, personal observations.

APPENDIX I

Species and mode examined

C, cDNA library; G, gross dissection; D, dentition; H, histology; M, magnetic resonance imaging.

Species	C	G	D	H	M
Atractaspinae					
Ambylodipsas polylepis		X	X		
Aparallactus lunulatus		X	X	X	
Atractaspis bibronii		X	X	X	
Colubridae					
Ahaetulla nasuta		X	X	X	
Boiga irregularis		X	X	X	
Chionactis occipitalis		X	X	X	
Chrysopelea ornate		X	X	X	
Coluber constrictor		X	X	X	
Crotaphopeltis hotamboeia		X	X	X	X
Dasypeltis scabra			X	X	X
Dispholidus typus	X	X	X	X	X
Lycodon aulicus		X	X	X	
Masticophis taeniatus		X	X	X	
Oligodon reticulatus			X	X	
Oligodon smithii		X	X		
Oxybelis aeneus		X	X	X	
Pantherophis guttata			X		X
Philothamnus irregularis		X	X	X	
Spalerosophis diadema			X	X	
Stenorrhina freminvillei		X	X	X	
Telescopus dhara	X		X		
Thelotornis capensis		X	X	X	
Micrurus fulvius		X	X	X	
Naja kaouthia			X		X
Naja melanoleuca		X	X	X	
Naja sputatrix		X	X	X	
Ophiophagus hannah		X	X		
Oxyuranus microlepidotus	X				
Pelamis platurus		X	X	X	
Walterinnesia aegyptia		X	X	X	
Homalopsidae					
Cerberus rynchops		X	X	X	X
Enhydris polylepis	X				
E. plumbea		X	X	X	
Erpeton tentaculatum		X	X	X	
Homalopsis buccata				X	
Lamprophiinae					
Lamprophis aurora		X	X	X	
Lycophidion capense			X	X	
Nactricidae					
Amphiesma stolatum		X	X	X	
Macropisthodon plumbicolor		X	X		
M. rudis			X		X
Nerodia sipedon		X	X	X	
Psammodynastes pulverulentus		X	X	X	
Regina septemvittata		X	X		
Rhabdophis tigrinus	X	X	X	X	

APPENDIX I—*continued*

Thrasops jacksonii	X				
Trimorphodon biscutatus	X	X	X	X	
Dipsadidae					
Carphophis amoenus				X	
Coniophanes fissidens		X		X	
Contia tenuis		X		X	
Diadophis punctatus		X	X	X	
Erythrolamprus aesculapii		X	X	X	
Helicops leopardinus			X	X	X
Heterodon nasicus		X	X	X	
Heterodon platyrhinos		X	X	X	
Hydrodynastes gigas		X	X	X	
Hypsiglena torquate		X	X	X	
Imantodes cenchoa		X	X	X	
Leptodeira annulata		X	X	X	
Liophis poecilogyrus	X				
Oxyrhopus petola		X	X	X	
Philodryas olfersii	X		X	X	
Pseudoboa neuwiedii			X	X	
Tachymenis peruviana		X	X	X	
Tomodon dorsatus		X	X	X	
Elapidae					
Aipysurus eydouxii		X	X	X	X
Aspidelaps lubricus		X	X		
Storeria occipitomaculata		X	X	X	
Thamnophis elegans		X	X	X	
Virginia valeriae		X	X	X	
Xenochrophis piscator		X	X	X	
Pareatidae					
Pareas carinatus			X	X	
Psammophiinae					
Malpolon monspessulanus		X	X	X	X
Psammophis mossambicus	X		X		X
P. schokari		X	X		
P. sibilans		X	X	X	
Psammophylax rhombeatus		X	X	X	
Pseudoxyrhophiinae					
Leioheterodon modestus		X			
L. madagascarensis	X				
Madagascarophis colubrinus		X	X	X	
Viperidae					
Azemiops feae	X	X	X	X	
Agkistrodon piscivorus		X	X	X	
Atheris squamigera		X	X	X	
Bitis arietans		X	X	X	
Bitis gabonica			X	X	X
Calloselasma rhodostoma		X	X		
Causus rhombeatus	X	X	X	X	

APPENDIX I—*continued*

Boulengerina annulata		X	X	X		*Cerastes vipera*		X	X	X	
Bungarus candidus		X	X	X		*Crotalus adamanteus*		X	X	X	
Calliophis bivirgata			X		X	*Crotalus atrox*		X	X	X	
Calliophis intestinalis		X	X			*Daboia russelli*		X	X		
Dendroaspis jamesonii			X		X	*Echis coloratus*		X	X	X	
Dendroaspis viridis		X	X	X		*Hypnale hypnale*		X	X	X	
Enhydrina schistose		X	X	X		*Porthidium ophryomegas*		X	X	X	
Hemachatus hemachatus		X	X	X		*Proatheris superciliaris*		X	X	X	
Hydrophis melanocephalus		X	X			*Sistrurus miliarius*		X	X		
Hydrophis melanoleuca			X	X		*Trimeresurus albolabris*			X	X	X
Lapemis curtus		X	X	X		*Vipera ammodytes*		X	X	X	

APPENDIX II

Structural variation

Epithelium: 1, no mucus; 2, isolated mucoid cells or patches; 3, prominent mucoid region or gland. Contour: 1, relatively large ovate duct; 2, duct diameter reduced, surrounded by extensive circular connective tissue; 3, internal partitions to venom duct. Vestibule: 1, no vestibule; 2, vestibule present adjacent to venom gland; 3, vestibule present adjacent to fang sheath; 4, vestibule in contact with oral cavity. Topography of venom duct opening: 1, venom duct opens only to oral cavity; 2, venom duct opens only to fang sheath; 3, venom duct opens to both oral cavity and fang sheath.

	Epithelium	Contour	Vestibule	Topography	Final Code
Atractaspinae					
Atractaspis bibroni	3	1	3	2	unique
Amblyodipsas polylepis	1	1	1	3	A
Aparallactus lunulatus	1	1	1	2	B
Colubridae					
Ahaetulla nasuta	1	1	1	3	A
Boiga irregularis	1	2	1	3	F
Chionactis occipitalis	1	1	1	2	B
Chrysopelea ornata	1	1	1	1	G
Coluber constrictor	2	1	1	1	H
Crotaphopeltis hotamboeia	1	1	1	3	A
Dispholidus typus	2	2	1	3	unique
Lycodon aulicus	2	1	4	1	unique
Masticophis taeniatus	2	1	3	2	unique
Oligodon sp?,	1	1	1	3	A
Oxybelis aeneus	1	1	3	2	I
Philothamnus irregularis	3	1	1	1	unique
Stenorrhina freminvillei	1	2	2	2	unique
Thelotornis capensis	1	2	1	3	F
Trimorphodon biscutatus	2	1	2	3	D
Dipsadidae					
Coniophanes fissidens	1	1	1	3	A
Contia tenuis	2	1	1	1	H
Diadophis punctatus	1	1	1	3	A
Erythrolamprus aesculapii	1	1	1	3	A
Heterodon nasicus	2	2	4	1	K
Heterodon platyrhinos	2	2	4	1	K
Hydrodynastes gigas	2	1	3	3	J
Hypsiglena torquata	1	1	3	2	I
Imantodes cenchoa	1	1	1	2	B
Leptodeira annulata	2	1	3	3	J
Oxyrhopus petola	1	1	1	2	B
Tachymenis peruviana	2	1	1	3	E
Tomodon dorsatus	3	1	3	3	unique
Elapidae					
Aipysurus eydouxii	3	3	3	2	L
Aspidelaps lubricus	3	3	3	2	L
Boulengerina annulata	3	3	3	2	L
Bungarus candidus	3	3	3	2	L

APPENDIX II—*continued*

	Epithelium	Contour	Vestibule	Topography	Final Code
Calliophis intestinalis	3	3	3	2	L
Dendroaspis viridis	3	3	3	2	L
Enhydrina schistosa	3	3	3	2	L
Hydrophis melanocephalus	3	3	3	2	L
Hemachatus haemachatus	3	3	3	2	L
Lapemis hardwickii	3	3	3	2	L
Micrurus fulvius	3	3	3	2	L
Naja melanoleuca	3	3	3	2	L
Naja sputatrix	3	3	3	2	L
Pelamis platurus	3	3	3	2	L
Ophiophagus hannah	3	3	3	2	L
Walterinnesia aegyptia	3	3	3	2	L
Homalopsidae					
Cerberus rynchops	1	1	3	3	C
Enhydris plumbea	1	1	2	2	unique
Erpeton tentaculatum	1	1	1	?	unique
Lamprophiinae					
Lamprophis aurora	1	1	3	3	C
Psammodynastes pulverulentus	3	1	1	2	unique
Natricidae					
Amphiesma stolatum	2	1	1	3	E
Macropisthodon plumbicolor	2	1	3	1	unique
Nerodia sipedon	2	1	1	2	unique
Regina septemvittata	1	1	2	3	unique
Rhabdophis tigrinus	2	1	2	3	D
Storeria occipitomaculata	1	1	1	1	G
Thamnophis elegans	2	1	1	3	E
Virginia valeriae					
Xenochrophis piscator	1	1	3	1	unique
Psammophiinae					
Malpolon monspessulanus	2	1	2	3	D
Psammophis schokari	2	1	3	3	J
Psammophis sibilans	2	1	3	3	J
Psammophylax rhombeatus	2	1	3	3	J
Pseudoxyrhophiinae					
Leioheterodon modestus	2	1	2	3	D
Madagascarophis colubrinus	2	1	1	3	E

APPENDIX II—*continued*

	Epithelium	Contour	Vestibule	Topography	Final Code
Viperidae					
Azemiops feae	3	3	3	2	L
Agkistrodon piscivorus	3	3	3	2	L
Atheris squamigera	3	3	3	2	L
Bitis arietans	3	3	3	2	L
Bitis gabonica	3	3	3	2	L
Calloselasma rhodostoma	3	3	3	2	L
Causus rhombeatus	3	3	3	2	L
Cerastes vipera	3	3	3	2	L
Crotalus adamanteus	3	3	3	2	L
Crotalus atrox	3	3	3	2	L
Daboia russelii	3	3	3	2	L
Echis coloratus	3	3	3	2	L
Hypnale hypnale	3	3	3	2	L
Proatheris superciliaris	3	3	3	2	L
Porthidium ophryomegas	3	3	3	2	L
Sistrurus miliarius	3	3	3	2	L
Trimeresurus albolabris	3	3	3	2	L
Vipera ammodytes	3	3	3	2	L

APPENDIX III
Dentitional morphology

Dentitional morphology categories are: 1) smooth surface and no enclosed venom canal; 2) no enclosed venom canal and surface with shallow furrow; 3) deep groove present but restricted to less than half the length of the tooth; 4) deep groove running the majority of the length of the tooth; 5) enclosed venom canal.

Atractaspidinae: *Amblyodipsas polylepis* (4), *Aparallactus lunulatus* (4), *Atractaspis bibroni* (5); **Colubridae**: *Ahaetulla nasuta* (3), *Boiga irregularis* (4), *Chionactis occipitalis* (4), *Chrysopelea ornata* (3), *Coluber constrictor* (1), *Crotaphopeltis hotamboeia* (4), *Dasypeltis scabra* (1), *Dispholidus typus* (3), *Lycodon aulicus* (1), *Masticophis taeniatus* (1), *Oligodon reticulatus* (1), *Oligodon smithii* (1), *Oxybelis aeneus* (4), *Pituophis guttatus* (1), *Philothamnus irregularis* (1), *Spalerosophis diadema* (1), *Stenorrhina freminvillei* (4), *Thelotornis capensis* (4), *Trimorphodon biscutatus* (3); **Dipsadidae:** *Carphophis amoenus* (1), *Coniophanes fissidens* (3), *Contia tenuis* (1), *Diadophis punctatus* (1), *Erythrolamprus aesculapii* (2), *Helicops leopardinus* (1), *Heterodon nasicus* (1), *Heterodon platyrhinos* (1), *Hydrodynastes gigas* (1), *Hypsiglena torquata* (1), *Imantodes cenchoa* (3), *Leptodeira annulata* (3), *Oxyrhopus petola* (3), *Philodryas olfersii* (4), *Pseudoboa neuwiedii (3)*, *Tachymenis peruviana* (3), *Tomodon dorsatus* (3); **Elapidae:** *Aipysurus eydouxii* (5), *Aspidelaps lubricus* (5), *Boulengerina annulata* (5), *Bungarus candidus* (5), *Calliophis bivirgata* (5), *Calliophis intestinalis* (5), *Dendroaspis jamesonii* (5), *Dendroaspis viridis* (5), *Enhydrina schistose* (5), *Hemachatus haemachatus* (5), *Hydrophis melanocephalus* (5), *Hydrophis melanoleuca* (5), *Lapemis curtus* (5), *Micrurus fulvius* (5), *Naja kaouthia* (5), *Naja melanoleuca* (5), *Naja sputatrix* (5), *Ophiophagus hannah* (5), *Pelamis platurus* (5), *Walterinnesia aegyptia* (5); **Homalopsidae**: *Cerberus rynchops* (3), *Enhydris plumbea* (3), *Erpeton tentaculatum* (3); **Lamprophiinae:** *Lamprophis aurora* (1), *Lycophidion capense* (1), *Psammodynastes pulverulentus* (3); **Natricidae:** *Amphiesma stolatum* (2), *Macropisthodon plumbicolor* (1), *Macropisthodon rudis* (1), *Nerodia sipedon* (1), *Regina septemvittata* (1), *Rhabdophis tigrinus* (1), *Storeria occipitomaculata* (1), *Thamnophis elegans* (1), *Virginia valeriae* (1), *Xenochrophis piscator* (1); **Psammophiinae:** *Malpolon monspessulanus* (4), *Psammophis mossambicus* (3), *Psammophis schokari* (3), *Psammophis sibilans* (3), *Psammophylax rhombeatus* (4); **'Pseudoxyrhophiinae'**: *Madagascarophis colubrinus* (3); **Viperidae:** *Azemiops feae* (5), *Agkistrodon piscivorus* (5), *Atheris squamigera* (5), *Bitis arietans* (5), *Bitis gabonica* (5), *Calloselasma rhodostoma* (5), *Causus rhombeatus* (5), *Cerastes vipera* (5), *Crotalus adamanteus* (5), *Crotalus atrox* (5), *Daboia russelli* (5), *Echis coloratus* (5), *Hypnale hypnale* (5), *Porthidium ophryomegas* (5), *Proatheris superciliaris* (5), *Sistrurus miliarius* (5), *Trimeresurus albolabris* (5), *Vipera ammodytes* (5).

* This work was supported by grants (to B. G. F.) from the Australian Academy of Science, Australian French Association for Science and Technology, Australia and Pacific Science Foundation, CASS Foundation, Ian Potter Foundation, International Human Frontiers Science Program Organisation, Netherlands Organisation for Scientific Research, and University of Melbourne (Faculty of Medicine and Department of Biochemistry) and a Department of Innovation, Industry and Regional Development Victoria Fellowship; by Australian Research Council Grant DP0451663 (to B. G. F. and J. A. N.); and by an Australian Government Department of Education, Science and Training/EGIDE International Science Linkages grant (to B. G. F., J. A. N., and N. V.). The costs of publication of this article were defrayed in part by the payment of page charges. This article must therefore be hereby marked "*advertisement*" in accordance with 18 U.S.C. Section 1734 solely to indicate this fact.

The nucleotide sequence(s) reported in this paper has been submitted to the GenBank™EBI Data Bank with accession number(s) EU029668–EU029765, EU036635–EU036637, and EU091709–EU091713.

§ To whom correspondence should be addressed. E-mail: bgf@unimelb.edu.au.

‖ Present address: Nestlé Research Center, Vers-chez-les-Blanc, P. O. Box 44, 1000 Lausanne, Switzerland.

REFERENCES

1. Vidal, N. (2002) Colubroid systematics: evidence for an early appearance of the venom apparatus followed by extensive evolutionary tinkering. *J. Toxicol. Toxin Res.* **21,** 21–41
2. Fry, B. G., Lumsden, N., Wüster, W., Wickramaratna, J., Hodgson, W. C., and Kini, R. M. (2003) Isolation of a neurotoxin (α-colubritoxin) from a 'non-venomous' colubrid: evidence for early origin of venom in snakes. *J. Mol. Evol.* **57,** 446–452
3. Fry, B. G., and Wüster, W. (2004) Assembling an arsenal: origin and evolution of the snake venom proteome inferred from phylogenetic analysis of toxin sequences. *Mol. Biol. Evol.* **21,** 870–883
4. Fry, B. G., Vidal, N., Norman, J. A., Vonk, F. J., Scheib, H., Ramjan, R., Kuruppu, S., Fung, K., Hedges, S. B., Richardson, M. K., Hodgson, W. C., Ignjatovic, V., Summerhayes, R., and Kochva, E. (2006) Early evolution of the venom system in lizards and snakes. *Nature* **439,** 509–632
5. Kardong, K. (1980) Evolutionary patterns in advanced snakes. *Am. Zool.* **20,** 269–282
6. Vidal, N., Delmas, A. S., David, P., Cruaud, C., Couloux, A., and Hedges, S. B. (2007) The phylogeny and classification of caenophidian snakes inferred from seven nuclear protein-coding genes. *C. R. Biol.* **330,** 182–187
7. Taub, A. M. (1967) Comparative histological studies on Duvernoy's gland of colubrid snakes. *Bull. Am. Mus. Nat. Hist.* **138,** 1–50
8. Gabe, M., and Saint Girons, H. (1969) Histological data on the salivary glands of the Lepidosauria. *Mém. Mus. Natn. Hist. Nat. Paris* **58,** 1–112
9. Kochva, E. (1978) Oral glands of the Reptilia, in *Biology of the Reptilia* (Gans, C., and Gans, K. A., eds) Vol. 8, pp. 43–161, Academic Press, New York
10. Young, B., and Kardong, K. (1996) Dentitional surface features in snakes (Reptilia: Serpentes). *Amphib.-Reptilia* **17,** 261–276
11. West, G. S. (1895) On the buccal glands and teeth of certain poisonous snakes. *Proc. Zool. Soc. Lond.* **1895,** 195–206
12. West, G. (1898) On the history of the salivary buccal and harderian glands of the colubroidae with notes on their tooth succession and the relationships of the poison ducts. *J. Linn. Soc. Lond. Zool.* **26,** 517–526
13. Sarkar, S. C. (1923) A comparative study of the buccal glands and teeth of the opisthoglypha, and a discussion on the evolution of the order from aglypha. *Proc. Zool. Soc. Lond.* **1923,** 295–322
14. Fry, B. G., Wüster, W., Ramjan, S. F. R., Jackson, T., Martelli, P., and Kini, R. M. (2003) LC/MS (liquid chromatography, mass spectrometry) analysis of Colubroidea snake venoms: evolutionary and toxinological implications. *Rapid Commun. Mass Spectrom.* **17,** 2047–2062
15. Huang, P., and Mackessy, S. P. (2004) Biochemical characterization of phospholipase A_2 (trimorphin) from the venom of the Sonoran Lyre Snake *Trimorphodon biscutatus lambda* (family Colubridae). *Toxicon* **44,** 27–36
16. Lumsden, N. G., Fry, B. G., Ventura, S., Kini, R. M., and Hodgson, W. C. (2005) Pharmacological characterisation of a neurotoxin from the venom of *Boiga dendrophila* (Mangrove snake). *Toxicon* **45,** 329–334
17. Lumsden, N. G., Banerjee, Y., Kini, R. M., Kuruppu, S., and Hodgson, W. C. (2007) Isolation and characterization of rufoxin, a novel protein exhibiting neurotoxicity from venom of the psammophiine *Rhamphiophis oxyrhynchus* (Rufous beaded snake). *Neuropharmacology* **52,** 1065–1070
18. Ching, A. T., Rocha, M. M., Paes Leme, A. F., Pimenta, D. C., de Fatima, M., Furtado, D., Serrano, S. M. T., Ho, P. L., and Junqueira de Azevedo, I. L. M. (2006) Some aspects of the venom proteome of the Colubridae snake *Philodryas olfersii* revealed from a Duvernoy's (venom) gland transcriptome. *FEBS Lett.* **580,** 4417–4422; Correction (2006) *FEBS Lett.* **580,** 5122–5123
19. Fry, B. G., Wüster, W., Kini, R. M., Brusic, V., Khan, A., Venkataraman, D., and Rooney, A. P. (2003) Molecular evolution of elapid snake venom three finger toxins. *J. Mol. Evol.* **57,** 110–129
20. Fry, B. G. (2005) From genome to 'venome': molecular origin and evolution of the snake venom proteome inferred from phylogenetic analysis of toxin sequences and related body proteins. *Genome Res.* **15,** 403–420
21. Nei, M., Gu, X., and Sitnikova, T. (1997) Evolution by the birth-and-death process in multigene families of the vertebrate immune system. *Proc. Natl. Acad. Sci. U. S. A.* **94,** 7799–7806
22. Harvey, A. L., Bradley, K. N., Cochran, S. A., Rowan, E. G., Pratt, J. A., Quillfeldt, J. A., and Jerusalinsky, D. A. (1998) What can toxins tell us for drug discovery? *Toxicon* **36,** 1635–1640
23. Menez, A. (1998) Functional architectures of animal toxins: a clue to drug design? *Toxicon* **36,** 1557–1572
24. Cushman, D. W., Ondetti, M. A., Gordon, E. M., Natarajan, S., Karanewsky, D. S., Krapcho, J., and Petrillo, E. W., Jr. (1987) Rational design and biochemical utility of specific inhibitors of angiotensin-converting enzyme. *J. Cardiovasc. Pharmacol.* **10,** S17–30
25. Chothia, C., and Lesk, A. M. (1986) The relation between the divergence of sequence and structure in proteins. *EMBO J.* **5,** 823–826
26. Greer, J. (1981) Comparative model-building of the mammalian serine proteases. *J. Mol. Biol.* **153,** 1027–1042
27. Guex, N., and Peitsch, M. C. (1997) SWISS-MODEL and the Swiss-PdbViewer: an environment for comparative protein modeling. *Electrophoresis* **18,** 2714–2723
28. Diemand, A. V., and Scheib, H. (2004) iMolTalk: an interactive, internet-based protein structure analysis server. *Nucleic Acids Res.* **32,** W512–W516
29. Koradi, R., Billeter, M., and Wuthrich, K. (1996) MOLMOL: a program for display and analysis of macromolecular structures. *J. Mol. Graph.* **14,** 51–55
30. Shikamoto, Y., Suto, K., Yamazaki, Y., Morita, T., and Mizuno, H. (2005) Crystal structure of a CRISP family Ca^{2+}-channel blocker derived from snake venom. *J. Mol. Biol.* **350,** 735–743
31. Wang, J., Shen, B., Guo, M., Lou, X., Duan, Y., Cheng, X. P., Teng, M., Niu, L., Liu, Q., Huang, Q., and Hao, Q. (2005) Blocking effect and crystal structure of natrin toxin, a cysteine-rich secretory protein from *Naja atra* venom that targets BKCa channel. *Biochemistry* **44,** 10145–10152
32. Yamazaki, Y., Brown, R. L., and Morita, T. (2002) Purification and cloning of toxins from elapid venoms that target cyclic nucleotide-gated ion channels. *Biochemistry* **41,** 11331–11337
33. Yamazaki, Y., and Morita, T. (2004) Structure and function of snake venom cysteine-rich secretory proteins. *Toxicon* **44,** 227–231
34. Yamazaki, Y., Koike, H., Sugiyama, Y., Motoyoshi, K., Wada, T., Hishinuma S., Mita, M., and Morita, T. (2002) Cloning and characterization of novel snake venom proteins that block smooth muscle contraction. *Eur. J. Biochem.* **269,** 2708–2715
35. Yamazaki, Y., Hyodo, F., and Morita, T. (2003) Wide distribution of cysteine-rich secretory proteins in snake venoms: isolation and cloning of novel snake venom cysteine-rich secretory proteins. *Arch. Biochem. Biophys.* **412,** 133–141
36. Harrison, R. A., Ibison, F., Wilbraham, D., and Wagstaff, S. C. (2007) Identification of cDNAs encoding viper venom hyaluronidases: cross-generic sequence conservation of full-length and unusually short variant transcripts. *Gene* (*Amst.*) **392,** 22–33
37. Chen, C., Hsu, C. H., Su, N. Y., Lin, Y. C., Chiou, S. H., and Wu, S. H. (2001)

Solution structure of a kunitz-type chymotrypsin inhibitor isolated from the elapid snake *Bungarus fasciatus*. *J. Biol. Chem.* **276,** 45079–45087
38. Drickamer, K. (1992) Engineering galactose-binding activity into a C-type mannose-binding protein. *Nature* **360,** 183–186
39. Komori, K., Konishi, M., Maruta, Y., Toriba, M., Sakai, A., Matsuda, A., Hori, T., Nakatani, M., Minamino, N., and Akizawa, T. (2006 May) Characterization of a novel metalloproteinase in Duvernoy's gland of *Rhabdophis tigrinus tigrinus*. *J. Toxicol. Sci.* **31,** 157–168
40. Lumsden, N. G., Fry, B. G., Kini, R. M., and Hodgson, W. C. (2004) In vitro neuromuscular activity of 'colubrid' snake venoms: clinical and evolutionary implications. *Toxicon* **43,** 819–827
41. Kamiguti, A. S., Theakston, R. D., Sherman, N., and Fox, J. W. (2000) Mass spectrophotometric evidence for P-III/P-IV metalloproteinases in the venom of the Boomslang (*Dispholidus typus*). *Toxicon* **38,** 1613–1620.
42. Brown, R. L., Lynch, L. L., Haley, T. L., and Arsanjani, R. (2003) Pseudechetoxin binds to the pore turret of cyclic nucleotide-gated ion channels. *J. Gen. Physiol.* **122,** 749–760
43. Brown, R. L., Haley, T. L., West, K. A., and Crabb, J. W. (1999) Pseudechetoxin: a peptide blocker of cyclic nucleotide-gated ion channels. *Proc. Natl. Acad. Sci. U. S. A.* **96,** 754–759
44. Guo, M., Teng, M., Niu, L., Liu, Q., Huang, Q., and Hao, Q. (2005) Crystal structure of the cysteine-rich secretory protein stecrisp reveals that the cysteine-rich domain has a K^+ channel inhibitor-like fold. *J. Biol. Chem.* **280,** 12405–12412
45. Kobayashi, K., Sasaki, T., Sato, K., and Kohno, T. (2000) Three-dimensional solution structure of ω-conotoxin TxVII, an L-type calcium channel blocker. *Biochemistry* **39,** 14761–14767
46. Mochca-Morales, J., Martin, B. M., and Possani, L. S. (1990) Isolation and characterization of helothermine, a novel toxin from *Heloderma horridum horridum* (Mexican beaded lizard) venom. *Toxicon* **28,** 299–309
47. Kini, R. M., Rao, V. S., and Joseph, J. S. (2001) Procoagulant proteins from snake venoms. *Haemostasis* **31,** 218–224
48. Rosenberg, H. (1967) Histology, histochemistry and emptying mechanism of the venom gland of some elapid snakes. *J. Morphol.* **122,** 133–156
49. Young, B., Blair, M., Zahn, K., and Marvin, J. (2001) Mechanics of venom expulsion in *Crotalus*, with special reference to the role of the fang sheath. *Anat. Rec.* **264,** 415–426
50. Young, B. A., Lee, C. E., and Daley, K. M. (2002) Do snakes meter venom? *Biosciences* **52,** 1121–1126
51. Young, B. A., Dunlap, K., Koenig, K., and Singer, M. (2004) The buccal buckle: the functional morphology of venom spitting in cobras. *J. Exp. Biol.* **207,** 3483–3494
52. Kochva, E., and Wollberg, M. (1970) The salivary glands of Aparallactinae (Colubridae) and the venom glands of *Elaps* (Elapidae) in relation to the taxonomic status of this genus. *Zool. J. Linn. Soc.* **49,** 217–224
53. Underwood, G., and Kochva, E. (1993) On the affinities of the burrowing asps *Atractaspis* (Serpentes: Atractaspididae). *Zool. J. Linn. Soc.* **107,** 3–64
54. Haas, G. (1973) Muscles of the jaw and associated structures in the Rhyncocephalia and Squamata, in *Biology of the Reptilia* (Gans, C., and Parsons, T., eds) Vol. 4, pp. 285–490, Academic Press, New York
55. Jansen, W., and Foehring, R. (1983) The mechanism of venom secretion from Duvernoy's gland of the snake *Thamnophis sirtalis* (Serpentes: Colubridae). *J. Morphol.* **175,** 271–277
56. Li, M., Fry, B. G., and Kini, R. M. (2005) Eggs only diet: the shift in preferred prey by the Marbled sea snake (*Aipysurus eydouxii*) resulting in a loss of postsynaptic neurotoxicity. *J. Mol. Evol.* **60,** 81–89
57. Li, M, Fry, B. G., and Kini, R. M. (2005) Putting the brakes on snake venom evolution: the unique molecular evolutionary patterns of *Aipysurus eydouxii* (Marbled sea snake) phospholipase A_2 toxins. *Mol. Biol. Evol.* **22,** 934–941
58. Keogh, J. S., Shine, R., and Donnellan, S. (1998) Phylogenetic relationships of terrestrial Australo-Papuan elapid snakes (subfamily Hydrophiinae) based on cytochrome b and 16S rRNA sequences. *Mol. Phylogenet. Evol.* **10,** 67–81
59. Vidal, N., Kindl, S. G., Wong, A., and Hedges, S. B. (2000) Phylogenetic relationships of xenodontine snakes inferred from 12S and 16S ribosomal RNA sequences. *Mol. Phylogenet. Evol.* **14,** 389–402
60. Vidal, N., and Hedges, S. B. (2002) Higher-level relationships of caenophidian snakes inferred from four nuclear and mitochondrial genes. *C. R. Biol.* **325,** 987–995
61. Lawson, R., Slowinski, J. B., Crother, B. I., and Burbrink, F. T. (2005) Phylogeny of the Colubroidea (Serpentes): new evidence from mitochondrial and nuclear genes. *Mol. Phylogenet. Evol.* **37,** 581–601
62. Ho, P. L., Soares, M. B., Yamane, T., and Raw, I. (1995) Reverse biology applied to *Micrurus corallinus*, a South American coral snake. *J. Toxicol. Toxin Rev.* **14,** 327–337
63. Rouault, M., Rash, L. S., Escoubas, P., Boilard, E., Bollinger, J., Lomonte, B., Maurin, T., Guillaume, C., Canaan, S., Deregnaucourt, C., Schrevel, J., Doglio, A., Gutierrez, J. M., Lazdunski, M., Gelb, M. H., and Lambeau, G. (2006) Neurotoxicity and other pharmacological activities of the snake venom phospholipase A_2 OS2: the N-terminal region is more important than enzymatic activity. *Biochemistry* **45,** 5800–5816
64. Gao, R., Kini, R. M., and Gopalakrishnakone, P. (2002) A novel prothrombin activator from the venom of *Micropechis ikaheka*: isolation and characterisation. *Arch. Biochem. Biophys.* **408,** 87–92